UNIVERSITY OF CENTRAL OKLAHOMA
Edmond, Oklahoma
GRADUATE COLLEGE

# FLOWS IN A ROTATING CYLINDER

A THESIS

SUBMITTED TO THE GRADUATE FACULTY

in partial fulfillment of the requirements for

the degree of

MASTER OF SCIENCE IN ENGINEERING PHYSICS

BY

TODOR I. IVANOV

Edmond, Oklahoma

2010

# FLOWS IN A ROTATING CYLINDER

A THESIS

APPROVED FOR THE DEPARTMENT OF ENGINEERING

AND PHYSICS

JUNE 2010

By David L. Martin

Weldon J. Wilson

# CONTENTS

TABLE OF FIGURES ..... iv
ABSTRACT OF THESIS ..... vi
1. LITERATURE REVIEW ..... 1
Hygrocysts ..... 1
Görtler Vortices ..... 1
Coordinates ..... 7
Notation: ..... 8
Boundary Conditions For Flow in The x Direction ..... 9
Notation for the Perturbations ..... 11
Solutions for the flow ..... 16
The Physical Nature of $\lambda$, a theorem by Jentzsch [12, p.298] ..... 17
Iteration Method for Finding the Lowest Eigenvalue ..... 19
Conclusion ..... 23
2. METHODS ..... 24
Discussion ..... 24
Apparatus ..... 25
a) The supporting frame ..... 25
b) Acrylic cylinder ..... 29
c) Stand for the motor ..... 30
Total Apparatus ..... 31
Advantages of the Apparatus: ..... 32
3. FINDINGS ..... 33
Gibbs Phenomenon in a Rotating Cylinder ..... 38
Centripetal Acceleration Effects on the Axial Stability of the Vortices ..... 41
Gravitational Interference by the Suspended Pool Water With the Boundary Layer ..... 45
Coriolis Effects Determine the Shape of the Flow Front ..... 49
Application ..... 52
SUMMARY ..... 54
REFERENCES ..... 55

# TABLE OF FIGURES

Figure 1. Taylor vortices forming in the annulus between two vertical cylinders, the inner one rotating with respect to the outer one [11]..... 3

Figure 2 Picture of Taylor vortices [20]..... 4

Figure 3 Picture of Taylor vortices [20]..... 4

Figure 4 Picture of Taylor vortices [20]..... 5

Figure 5. Görtler vortices over a concave wall: λ is the wavelength of the vortex, δ is the boundary layer thickness, R is the radius of curvature of the plate [4]. 5

Figure 6. Up- and down-wash regions [4] ..... 6

Figure 7. Free stream velocity profiles for up-wash and down-wash regions [15] ..... 6

Figure 8 First view of the Görtler's vortices from the rising side of a 3" cylinder (follow the suspended air bubbles in the water) 3", 5/10, 580 RPM, the arrow shows the Up-wash region, there a stream of bubbles is carried by the up-wash to the surface..... 7

Figure 9 Graph of the results from Eqs. 43.1 for $v = 2,3,4$ for the straight line velocity profile as a function of σ [10]. $\mu 2(\sigma)$ is the Görtler number $\mu 2 = U0\delta\ v\delta R \equiv$ Gö. For $\sigma$ see (18),(19) $\sigma = \alpha\delta = 2\pi\delta\lambda$. ..... 22

Figure 10. Left view of supporting frame and cylinder..... 26

Figure 11. Right symmetrical view of supporting frame and cylinder..... 26

Figure 12. Detail of groove and hole. Such fastening allows for the horizontal bar to fit flush against the inside of the vertical bar..... 26

Figure 13. Front view of cylinder and the supporting frame ..... 27

Figure 14. Groove and hole allows vertical flush fit and utilizes the concept from the Vernier caliper with the smallest increment for hole and groove alingment of .2"..... 27

Figure 15. Sliding assembly ..... 27

Figure 16 View of one of the ends of the sliding assembly attached with a bolt to the fixed rail. The fixed rail has the thicker border..... 28

Figure 17 From left to right: lid away from motor, cylinder, lid toward the motor, and the lid that fits over the pulley and bolts to the cylinder lid that is toward the motor, all units in (in.) ..... 29

Figure 18. Motor and its base..... 30

Figure 19. Adjustable base for the motor, all units in (in.) ..... 30

Figure 20. Complete apparatus, side view, ..... 31

Figure 21. The complete apparatus, view opposite from the motor ..... 31

Figure 22. Angled side view, of the sliding assemblies, fixed rails, motor, motor frame, cylinder, and lids..... 32

Figure 23 Difference in concentricity of inner and outer edge for the 3” cylinder ..... 37

Figure 24. Gibbs phenomenon 2 terms [19]..... 38

Figure 25. Gibbs phenomenon 16 terms (note the 16 half wavelengths) [19] 39

Figure 26 End view of the Gibbs phenomenon in a cylinder with an aspect ratio of ~10, 5/10 fill-volume, (extracted from video)..... 40

Figure 27 Line-fit for various fill-volumes for a 3” cylinder not affected by the gravitational effects of the pool of water over the boundary layer ..... 42

Figure 28 Line-fit for various fill-volumes for a 5” cylinder not affected by the gravitational effects of the pool of water over the boundary layer ..... 43

Figure 29 Line-fit for various fill-volumes for a 7” cylinder not affected by the gravitational effects of the pool of water over the boundary layer ..... 44

Figure 30. Picture of a small pool of water standing over the boundary layer (7”, 4/10, 444 RPM). The angular velocity is into the picture. The boundary layer is visualized by the water at the rising end of the cylinder. The color scheme of the picture has been altered to improve visibility. ..... 46

Figure 31. The standing pool of water over the narrow boundary layer, 7” cyl. 7/10 full, 320 RPM, (the picture is extracted from a video). The angular velocity is into the picture. The color scheme of the picture has been altered to improve visibility. ..... 47

Figure 32. The standing pool of water over the narrow boundary layer , 7” cyl., 7/10 full, 303 RPM. The angular velocity is into the picture. The color scheme of the picture has been altered to improve visibility. ..... 48

Figure 33. Shark teeth, high dynamic viscosity, rotating at 3.2 rpm, dynamic viscosity $\mu = 49$ cp, fill-fraction 6% [14]..... 49

Figure 34. Picture of the surface formed at low rotational rates and low water volume fraction (7”, 417 RPM). The color scheme of the picture has been altered to improve visibility. ..... 50

Figure 35. The Coriolis force pushes the down-wash regions in direction opposite of the tangential velocity (upstream) ..... 51

Figure 36. The Coriolis force pulls the up-wash regions downstream ..... 52

# ABSTRACT OF THESIS

University of Central Oklahoma

Edmond, Oklahoma

NAME: Ivanov, Todor

TITLE OF THESIS: FLOWS IN A ROTATING CYLINDER

DIRECTOR OF THESIS: David L. Martin

PAGES: 66

ABSTRACT:

The purpose of this work is to focus on studying Görtler vortices inside a rotating cylinder. The literature review chapter, (Chapter 1), gives us insight from Görtler and Hämmerlin on the dominant - centrifugal and viscous forces. Their theoretical work inspired the hypothesis of this paper that for a fixed volume-fill, and diameter cylinder, there is a discrete set of tangential speeds of rotation when the Görtler vortices become axially stable. Or, equivalently, that the down-wash regions of the vortices do not move along the z-axes . In the Findings chapter we will discuss what we have discovered on how the coriolis effects shape the flow front for a cylinder with a low fill-volume fraction. The gravitational effects from the suspended over the boundary layer pool can not be ignored for cylinder fill-volumes of 7/10, 8/10 and 9/10 fill. The axial end effects are linked to the existence of a Gibbs phenomenon in a whole section in Chapter 3.

Two flow phenomena are described in the literature:

- Hygrocysts- sheets of water that form along the z-axes [2]
- "Shark teeth"- for a low fill volume fraction, the flow front takes on periodically varying in axial direction angular values. [14]

We will link the above two flow phenomena to a common underlying cause: the Görtler vortices. The first resulting from strong vortices and the second from a coriolis force. We will introduce the hypothesis that for some values of the tangential speed of rotation the vortices stop shifting axially and become axially fixed (along the z-axis). That makes the axially unstable vortices the far more common event in the domain of tangential speeds for a finite rotating cylinder.

The Literature Review (Chapter 1) answers the question if there is a lower limit on the tangential speed of rotation for the vortices first to appear. This is the main question answered by the Hämmerlin's 1955 paper. It will show that the vortices exist even for very low free stream velocity (Görtler number). The overview of Hämmerlin's breakthrough solution on the Görtler problem is covered exclusively in Chapter 1 since it is the most detailed theoretical work concerning the vortices (according to Görtler ). Hämmerlin solves a system of coupled non-adjoint differential equations for the value of a common parameter. That parameter describes when the two coupled equations have a joint solution. The algorithm is by H. Wielandt from 1944 [7]. The algorithm gives the common parameter as a function of the other dimensionless number in the system, Eqs. 28, 29. The graph of the Görtler number as a function of the other dimensionless number is on Figure 9. The three curves on that figure

result from different levels in the iteration algorithm. At the end Hämmerlin shows that the parameter does not take on a positive local minimum within the approximations that he used to simplify the original Navier-Stokes' equations. He also includes a section on why the parameter (Görtler number) cannot take on negative values.

We then will use the air bubbles that incorporate in the water to visualize and record the action of the vortices under the surface. We will find experimentally that axially stable vortices exist for a given: cylinder curvature, tangential speed of rotation, and fill-volume fraction. There is a whole section in Chapter 3 on the gravitational effects, of the suspended pool of water over the boundary layer.

This paper will link the vortices to a coriolis force that determines the shape of the flow front for low fill-volume fractions, Chapter 3. Hämmerlin's work for a flow over a concave wall is also valid for the case of an axially infinite cylinder, compare with Bottaro [16]. We will show experimentally that "Hygrocysts", or sheets of water originate from the down-wash regions.

I want to thank Dr. Martin for his interest in the work and willingness to work with me.

# 1. LITERATURE REVIEW

Hygrocysts

According to Balmer the phenomenon of forming of vertical discs of liquid in a horizontally rotating cylinder has been overlooked [2]. He reports that his paper is the first study on the subject. The author gives it the name "Hygrocyst".

Görtler Vortices

Here is the form of the Görtler number: $\text{Gö} = Re\sqrt{\frac{\delta}{R}}$, $(Re = \frac{U_0\delta}{v})$, where $\delta$ is the boundary layer thickness, $v$ is the kinematic viscosity, and $R$ is the radius of curvature. Zebib and Bottaro in their 1993 paper expanded the scope of the computations to include also a coriolis term from the Navier-Stokes equations in their calculations [16]. Their solution method is more contemporary yet it lacks the physical insight that gives the work of a doctorial student of Görtler by the name of G. Hämmerlin that was also presented to the German Academy of Sciences personally by H. Görtler.

For the case of pure Görtler vortices (influenced only by viscous and centrifugal forces) the ratio of boundary layer thickness to radius of curvature of the cylinder has to be very small. The centrifugal and viscous forces dominate the flow. Hämmerlin limited the four Navier-Stokes equations to only two and forced both of the equations to depend on a single parameter. Görtler

created the Green's functions that transformed the system of non-adjoint coupled differential equations into a system of coupled integral equations.

There is also a discussion in Chapter 3 of this paper on the coriolis effects of the vortices. It was inspired by the coriolis term that Zebib and Bottaro included in their paper [16] and a picture by Thoroddsen showing the effects of higher dynamic viscosity on the shape of the flow front, Figure 33. The reason for the review of Hämmerlin's paper is Görtler's 1955 paper highlighting the need for studying these very destructive vortices, where he also recommended the work of Günter Hämmerlin [8,10]. There was a very large discrepancy (orders of magnitude difference) between the results of Görtler and Meksyn [pg. 287, 10]. Meksyn's error in solving a system of coupled differential equations was in choosing a constant velocity profile that erases the RHS of a differential equaton, Eq. (25), [10]. The error is magnified by adding a third equation that is simply a derivative of Eq. (26), [10]. Meksyn's final results differed orders of magnitude from the Görtler's. Hämmerlin's paper in 1955 settled this dispute by showing that a system of coupled differential equations where one depends on a parameter and the eigenvalues of that parameter are the topic of study, then the other of the coupled differential equations must be forced to also depend on the same parameter. He uses a major solution algorithm by H. Wielandt [7,10] The work on the forming of vortices between two concentric vertical cylinders was first quantized by Rayleigh and later by G.I. Taylor in cylindrical coordinates, that required a lot of Bessel functions [13].

Görtler‘s vortices, in a partially filled horizontally rotating cylinder, differ from the Taylor-Coyette vortices in that there is no limitation on the maximum height of the boundary layer (diameter of the vortices). The Taylor-Coyette flow has the advantage of allowing a greater free-stream velocity, defined to be the difference between the speed of the liquid at the top and bottom of the boundary layer.

Görtler’s vortices were unforeseeable by the two-dimensional models of Tollmien and Schlichting [26]. Görtler applied the Navier-Stokes equations to the horizontal flow over slightly concave surface. The vortices that emerge are not present in the flow over a flat plate. With increase in the free stream velocity the effects of vortices in creating a wavy flow front become noticable. The vortices’ rotation axes are in direction of the free stream velocity. There are similarities with Taylor’s vortices:

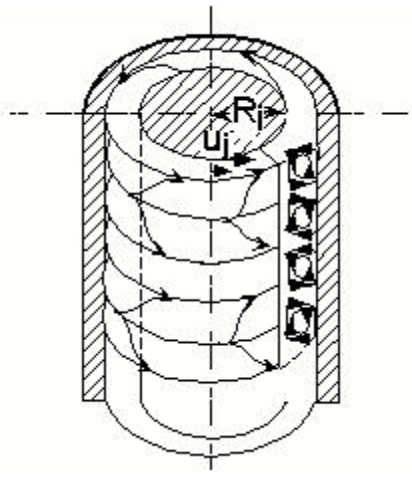


Figure 1. Taylor vortices forming in the annulus between two vertical cylinders, the inner one rotating with respect to the outer one [11]

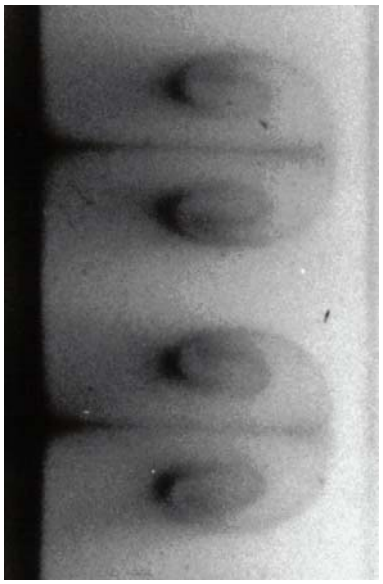

Figure 2 Picture of Taylor vortices [20]

Figure 3 Picture of Taylor vortices [20]

The figure is in full agreement with Figure 1. The down-wash regions are at the round spots and the inward cusped spots are the up-wash regions.

Figure 4 Picture of Taylor vortices [20]

These are more powerful vortices at a higher angular velocity of the inner cylinder. Note the longer vortex wavelength, since it took only 7 down-wash regions (Figure 4) to fill the whole cylinder where earlier there could fit 10 (Figure 3).

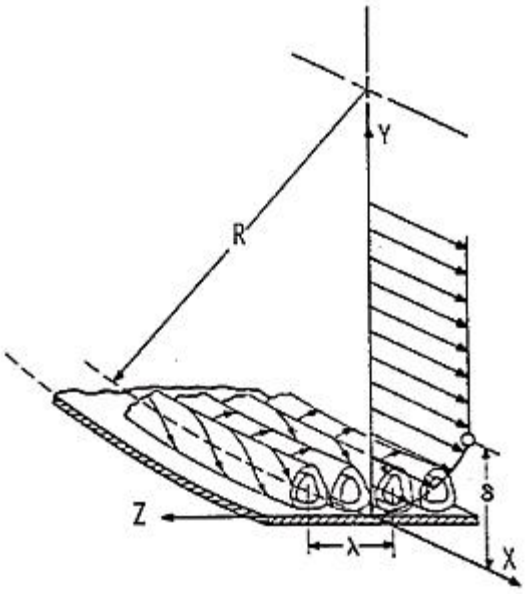


Figure 5. Görtler vortices over a concave wall: λ is the wavelength of the vortex, δ is the boundary layer thickness, R is the radius of curvature of the plate [4]

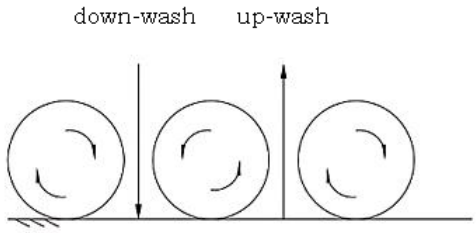


Figure 6. Up- and down-wash regions [4]

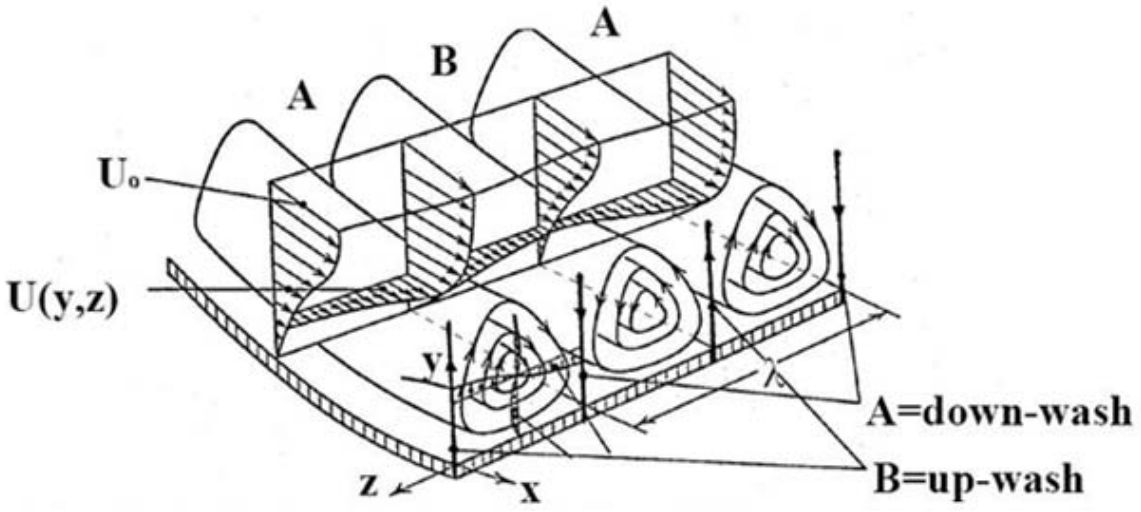


Figure 7. Free stream velocity profiles for up-wash and down-wash regions [15]

All of the drown velocity profiles are for the velocity component in the *x* direction and they are a function of the radial distance from the concave surface. Typically the problem was described through cylindrical coordinates and with Bessel functions, [13]. To describe the time-independent fully developed flow, Görtler used rectangular coordinates with a fixed on the concave surface origin.

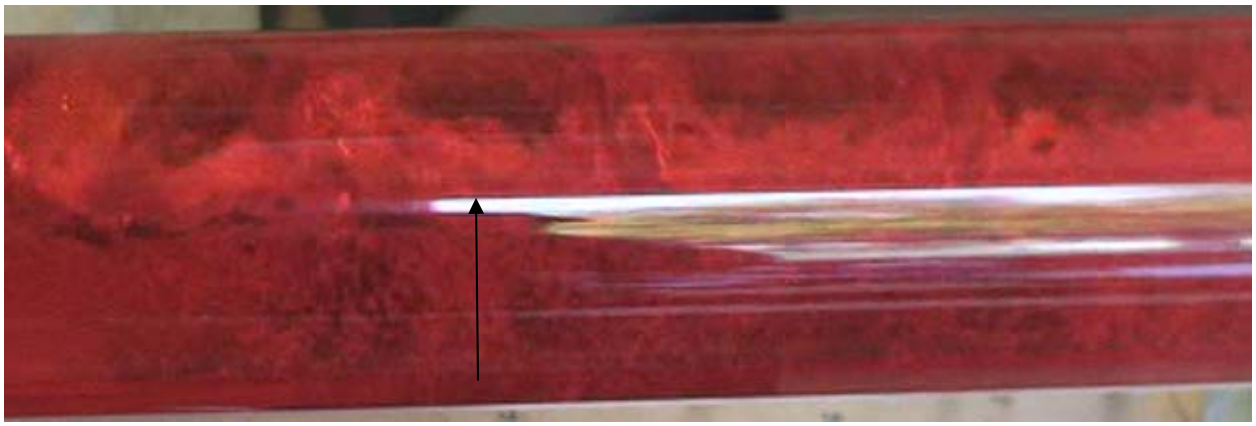

Figure 8 First view of the Görtler's vortices from the rising side of a 3" cylinder (follow the suspended air bubbles in the water) 3", 5/10, 580 RPM, the arrow shows the Up-wash region, there a stream of bubbles is carried by the up-wash to the surface.

In 1950 Meksyn published a work on the Görtler problem. His results for a local minimum of the curve fit that connects the discrete calculated values for the Görtler number were orders of magnitude higher than those of Görtler from 1940. The difference could not be attributed to an error from the approximations [10, p.287]. Then H. W. Liepmann tried, yet unsuccesfully, to verify experimentally either of the results. Then Hämmerlin applied a method by H. Wielandt from 1944 on solving eigenvalue problems for a system of coupled non-adjoint differential equations for the values of a common (to both equations) parameter [7]. He showed that Görtler's results to a slight approximation were correct [10]. From here on till the end of Chapter 1 follows a brief overview of Hämmerlin's paper.

Coordinates

Here follow the Navier-Stokes' equations in rectangular coordinates for a steady state incompressible flow, that is not disturbed by gravity.

$$\rho\left(u_t + uu_x + \vartheta u_y + \omega u_z\right) = -p_x + \mu\left(u_{xx} + u_{yy} + u_{zz}\right), \quad 1$$

$$\rho\left(\vartheta_t + u\vartheta_x + \vartheta\vartheta_y + \omega\vartheta_z\right) = -p_y + \mu\left(\vartheta_{xx} + \vartheta_{yy} + \vartheta_{zz}\right), \quad 2$$

$$\rho\left(\omega_t + u\omega_x + \vartheta\omega_y + \omega\omega_z\right) = -p_z + \mu\left(\omega_{xx} + \omega_{yy} + \omega_{zz}\right). \quad 3$$

Here also follows the Continuity equation, 4

$$u_x + \vartheta_y + \omega_z = 0. \quad 5$$

The coorinate system used by Hämmerlin is a rectangular one fixed on the concave surface, Figure 7. Hämmerlin uses ($R > 0$) to describe a concave surface. In the above coordinate orientation follows the first of the Navier-Stokes equations:

Notation:

- $u, \vartheta, \omega$ –velocity components in x,y,$z$ directions
- $p$ –pressure
- subscripts at first will denote derivatives with respect to
- $\rho$ –density (constant, non-compressible liquid, no incorporation of bubbles)
- $v$ –kinematic viscosity (constant, ignore heating or cooling effects)
- $U$ –will stand for free stream velocity

Schlichting first gives the form of the Navier-Stokes' equations that appers in Eq. 6 [26, pg. 163, pg. 166]. Görtler uses Schlichting's transformations without going into any detail [27, pg. 139]:

Note: The angular direction of a cylindrical coordinate system fixed at the center of curvature coincides with the $x$ direction for a rectangular coordinate system fixed on the concave surface a distance $R$ from the center of curvature.

$$u_t + \frac{R}{R-y}uu_x + \vartheta u_y - \frac{u\vartheta}{R-y} + \omega u_z = -\frac{R}{R-y}\frac{1}{\rho}p_x + v\left\{\frac{R^2}{[R-y]^2}u_{xx} + u_{yy} + u_{zz} - \frac{1}{R-y}u_y - \frac{2R}{[R-y]^2}\vartheta_x - \frac{u}{[R-y]^2}\right\} \quad (6)$$

This is the first of the Navier-Stokes' equations and is taken directly from Görtler, [9]. Similar equations exist for the flow in the $y$ and $z$ directions and also for the continuity. Görtler developes $\frac{1}{R-y}$ and $\frac{R}{R-y}$ in powers of $\frac{y}{R}$, and keeps only terms with denominator less than $R^2$, since $R$ is big, so $\frac{1}{R-y} \approx \frac{1}{R}$, and $\frac{R}{R-y} \approx 1 + \frac{y}{R}$, [9].

Boundary Conditions For Flow in The x Direction

$$u_x = \vartheta_x = 0$$

These are the result from him studying fully developed flow. The strength of the vortices does not vary with angular position on the concave surface. In other words the vortex wavelength is constant since increasing wavelength corresponds to stronger vortices. Since a pressure difference is not the driving factor behind the vortices then:

$$p_x = 0.$$

Here are the steps that Hämmerlin follows:

- Substituting in Eq. 6 the above boundary conditions and the series expansions
- Retains only the terms with denominator smaller than $R^2$.
- The series expansions introduce terms $\frac{u_y}{R}, \frac{v_y}{R}, \frac{w_y}{R}$ that are orders of magnitude smaller than $u_{yy}, v_{yy}, w_{yy}$ , so they are dropped at this level of approximation , (since $u_{yy} \sim \frac{u_y}{y}$, $y \leq \delta$, and $\delta \ll R$). Here the boundary layer thickness $\delta$ is a fixed quantity.

After these approximations Hämmerlin obtains the following system of partial differential equations:

$$u_t + \vartheta u_y - u\vartheta\frac{1}{R} + \omega u_z = v\left(u_{yy} + u_{zz}\right),$$

$$\vartheta_t + \vartheta\vartheta_y + \frac{u^2}{R} + \omega\vartheta_z = -\frac{1}{\rho}p_y + v\left(\vartheta_{yy} + \vartheta_{zz}\right), \qquad 7$$

$$\omega_t + \vartheta\omega_y + \omega\omega_z = -\frac{1}{\rho}p_z + v\left(\omega_{yy} + \omega_{zz}\right),$$

$$\vartheta_y + \omega_z = 0.$$

The first three were the Navier-Stokes' equations and the last one is the Continuity equation. Hämmerlin introduces the following slight perturbations. The perturbed quantities have a subscript 1 , and the unperturbed, the subscript 0. The unperturbed solution is for laminar flow and the perturbations will describe mathematically the vortices.

Notation for the Perturbations

- $\alpha = \frac{2\pi}{\lambda}$ is the wave number, and $\lambda$ is the vortex wavelength, Figure 5, Figure 7. Here is the last place where $\lambda$ stands for wavelength. Later $\lambda$ will be just a parameter to keep the standard notation for the Fredholm integral equations.
- $p_0(y), u_0(y)$ are a solution for a completely laminar flow. All other expressions on the RHS of the perturbations 8 describe the vortices from Figure 7. $u_1(\mathrm{y}), \vartheta_1(\mathrm{y})$, and $\omega_1(\mathrm{y})$ are small compared to $p_0(y), u_0(y)$.

$$\begin{aligned} u &= u_0(y) + u_1(\mathrm{y})\cos(\alpha z)\cdot e^{\beta t} \\ \vartheta &= \vartheta_1(\mathrm{y})\cos(\alpha z)\cdot e^{\beta t} \\ \omega &= \omega_1(\mathrm{y})\sin(\alpha z)\cdot e^{\beta t} \\ p &= p_0(y) + p_1(\mathrm{y})\cos(\alpha z)\cdot e^{\beta t}. \end{aligned} \qquad 8$$

The above expressions describe the flow with the origin chosen at the center of a down-wash region, Figure 7 . Apply the perturbations 8 to Eqs. 7 and ignore any term with a product of two of the three: $u_1(\mathrm{y}), \vartheta_1(\mathrm{y}),$ or $\omega_1(\mathrm{y})$, one obtains:

$$\beta u_1 + \vartheta_1 \frac{\partial u_0}{\partial y} = v\left(\frac{\partial^2 u_1}{\partial y^2} - \alpha^2 u_1\right) \qquad 9$$

$$\beta \vartheta_1 + u_1 \frac{2u_0}{R} + \frac{1}{\rho}\frac{\partial p_1}{\partial y} = v\left(\frac{\partial^2 \vartheta_1}{\partial y^2} - \alpha^2 \vartheta_1\right) \qquad 10$$

$$\beta \omega_1 - \frac{\alpha}{\rho} p_1 = v\left(\frac{\partial^2 \omega_1}{\partial y^2} - \alpha^2 \omega_1\right) \qquad 11$$

$$\omega_1 = -\frac{1}{\alpha}\frac{\partial \vartheta_1}{\partial y}. \qquad 12$$

Substituting Eq. 12 in Eq. 11, he gets an expression for $p_1$and then he subsitutes that in for $p_1$ , Eq. 10. The substitution leads to only two non-adjoint equations. After simplifying and collecting terms, he gets:

$$v\frac{\partial^4\vartheta_1}{\partial y^4}-(2\alpha^2 v\ +\ \beta)\frac{\partial^2\vartheta_1}{\partial y^2}+\alpha^2(\beta+v\alpha^2)\vartheta_1=-\frac{2\alpha^2 u_0}{R}u_1. \tag{13}$$

Eq. 9 is unchanged:

$$v\frac{\partial^2 u_1}{\partial y^2}-(\alpha^2 v+\beta)u_1=\vartheta_1\frac{\partial u_0}{\partial y}. \tag{14}$$

Hämmerlin changes to the dimensionless variables shown:

$$\eta=\frac{y}{\delta}\ ,y=\eta\delta\ ,dy=\delta d\eta$$
$$U=\frac{u_0}{U_0},u_0=U\ U_0 \tag{15}$$

where $\delta$ is the height of the boundary layer, is constant and approximately equal to half a wavelength Figure 7.

Substituting $\eta$ and $U$ into the Equations (20) and multyplying out the constants in front of the highest derivative in each equation, gives:

$$\frac{\partial^4\vartheta_1}{\partial\eta^4}-\left(2\alpha^2\delta^2\ +\ \frac{\beta\delta^2}{v}\right)\frac{\partial^2\vartheta_1}{\partial\eta^2}+\alpha^2\delta^2\left(\alpha^2\delta^2+\frac{\beta\delta^2}{v}\right)\vartheta_1=-\frac{2\alpha^2\delta^4 U\ U_0}{vR}u_1 \tag{16}$$

$$\frac{\partial^2 u_1}{\partial\eta^2}-\left(\alpha^2\delta^2+\frac{\beta\delta^2}{v}\right)u_1=\frac{U_0\delta\vartheta_1}{v}\frac{\partial U}{\partial\eta}. \tag{17}$$

The dimensionless constants that he introduces in Eqs. (18,19,20,21,22) change the form of Eqs. (16,17) into the form of Eqs. (23,24):

$$\sigma=\alpha\delta,\alpha=\frac{\sigma}{\delta},\left(\alpha=\frac{2\pi}{\lambda}\right), \tag{18}$$

where $\delta$ is constant, and is the maximum height of the boundary layer. Here $\lambda$ still stands for the wave length, see Figure 7, Figure 33, Figure 34.

$$\tau = \sqrt{\left(\alpha^2\delta^2 + \frac{\beta\delta^2}{v}\right)} = \sqrt{(\sigma^2 + \frac{\beta\delta^2}{v})}\,, or\ \tau^2 = \alpha^2\delta^2 + \frac{\beta\delta^2}{v} = \sigma^2 + \frac{\beta\delta^2}{v} \qquad 19$$

$$\mu = 2\left(\frac{U_0\delta}{v}\right)^2 \frac{\delta}{R}\,, so\ \sqrt{\frac{\mu}{2}} = Re\sqrt{\frac{\delta}{R}} \equiv \text{Gö} \qquad 20$$

$Re$ is the boundary layer Reynolds number. For a cylinder $U_0$ is the tangential speed of the inner edge, since that is also the speed of the flow front. The mathematics are for an axially infinite concave surface, or an axially infitite rotating cylinder Figure 7. The primed notation that follows is for new dimensionless variables and not for differentiation, differentiation is still shown with subscripts.

$$u' = \frac{u_1}{\left(\frac{U_0\delta}{v}\right)} \quad or \quad u_1 = \left(\frac{U_0\delta}{v}\right) u', du_1 = \left(\frac{U_0\delta}{v}\right) du' \qquad 21$$

$$\vartheta' = \vartheta_1, d\vartheta_1 = d\vartheta'. \qquad 22$$

Note: The SI units of kinematic viscosity $v$ are $m^2 \cdot s^{-1}$, $\alpha$ has units of $m^{-1}$, and $\beta$ has $s^{-1}$.

Substitute (18) and (19) in (16) and (17), then use (20) and (21) to simplify and again return to unprimed notation for $u$ and $v$, so the primes again stand for derivatives with respect to $\eta$ like in (16) and (17)

$$u'' - \tau^2 u = \vartheta\frac{\partial U}{\partial \eta}, \qquad 23$$

$$\vartheta'''' - (\tau^2 + \sigma^2)\vartheta'' + \tau^2\sigma^2\vartheta = -\mu\sigma^2 U u. \qquad 24$$

Fully developed flow is most important and that is the one he solves for:($\beta = 0$, or equivalently $\tau = \sigma$).

The time-independent equations become:

$$u'' - \sigma^2 u = \vartheta \frac{\partial U}{\partial \eta} \tag{25}$$

$$\vartheta'''' - 2\sigma^2 \vartheta'' + \sigma^4 \vartheta = -\mu \sigma^2 U u. \tag{26}$$

These equations were also used by Meksyn yet his solution involved a constant velocity profile that is contrary to Boundary Layer Theory. He used that velocity profile to turn Eq. (25) into a homogeneous equation, thus destroying the coupling of the Eqs. (25) and (26) [10]. $U$ is a function of $\eta$, since $U_0$ is a constant, $u_0 = u_0(y)$, $y = \eta\delta$, and $U = \frac{u_0}{U_0}$, so $\frac{\partial U}{\partial \eta} = \frac{1}{U_0}\frac{\partial u_0}{\partial \eta}$. Here $\delta$ is a constant, since the vortex wavelength is set constant, as in see Figure 5. Later in determining meaningful expressions for the velocity profiles for $U$ Figure 7 will be very important. The focus of study is again the point of change from laminar flow to flow with vortices over an axially-infinite concave surface, or axially infinite rotating cylinder. From here on $\lambda$ will be just a paramenter (dimensionless number), to fit the standard notation for the Fredholm integral equation of the second kind. It will be clarified if $\lambda$ takes on again the meaning of wavelength like it did in (18):

$$\mu^{\frac{1}{2}} = \lambda, \;\; \mu = \lambda^2, \tag{27}$$

$\lambda$ here is just a parameter, multiple of Gö incorporating the 2 from the RHS of Eq. 16. $\lambda$ is not the wavelength from Figure 5, and Figure 7. It is the dimensionless number $\lambda = \sqrt{\mu} = \sqrt{2}\text{Gö} = \sqrt{2}Re\sqrt{\frac{\delta}{R}}$, (20).

He rewrites $u$ as $\lambda u$ to include the parameter also in the RHS of Eq. 25. In this form after simplifying he makes both equations to depend on a single parameter:

$$u'' - \sigma^2 u = \lambda \frac{\partial U}{\partial \eta}\vartheta \qquad 28$$

$$\vartheta'''' - 2\sigma^2\vartheta'' + \sigma^4\vartheta = -\lambda\sigma^2 U u. \qquad 29$$

This set of equations is unique to Hämmerlin's paper. Equations (28, 29) are important since they show the time independent behavior. We will be looking at the eigenvalues $\lambda$ of the system formed by Eqs. (28, 29). The boundary conditions,

$$u(0) = \vartheta(0) = 0$$

follow from Boundary Layer Theory. The boundary condition,

$$\vartheta'(0) = 0$$

follows from Eq. 12 and is equivalent to $\omega_1(0) = 0$.

The boundary conditions (30) stand for the fact that high enough over the concave surface there is no flow and there are no vortices,

$$u(\infty) = \vartheta(\infty) = \vartheta'(\infty) = 0. \qquad 30$$

Solutions for the flow

The following Green's functions were developed by Görtler. Unlike the series expansions that Görtler used in his 1940 paper. These Green's functions guarantee completeness of the set of solutions. The transformed LHS's of the Eqs. (25) and (26) follow through Green's functions into kernels of integral equations. $\tau = \sigma$ means a time independent solution for the fully developed flow:

$$G(\eta, \eta_0) = \frac{1}{\sigma} e^{-\sigma\eta_0} \sinh \sigma\eta \qquad for\ \eta \le \eta_0 \qquad 31$$

$$G(\eta, \eta_0) = \frac{1}{\sigma} e^{-\sigma\eta} \sinh \sigma\eta_0 \qquad for\ \eta_0 \le \eta \qquad 32$$

$$H(\eta, \eta_0) = \frac{1}{4\sigma^3}\left[e^{-\sigma(\eta_0+\eta)}\{2\sigma^2\eta_0\eta + \sigma(\eta_0+\eta) + 1\}\right.$$
$$\left. - e^{-\sigma(\eta_0-\eta)}\{\sigma(\eta_0-\eta) + 1\}\right] \qquad for\ \eta \le \eta_0 \qquad 33$$

$$H(\eta, \eta_0) = \frac{1}{4\sigma^3}\left[e^{-\sigma(\eta+\eta_0)}\{2\sigma^2\eta\eta_0 + \sigma(\eta+\eta_0) + 1\}\right.$$
$$\left. - e^{-\sigma(\eta-\eta_0)}\{\sigma(\eta-\eta_0) + 1\}\right]. \qquad for\ \eta_0 \le \eta \qquad 34$$

Then the coupled Equations (28, 29) can be transformed in coupled integral equations with kernels $H(\eta, \eta_0)$ and $G(\eta, \eta_0)$.

$$u(\eta) = -\lambda \int_0^\infty G(\eta, \eta_0) \frac{dU(\eta_0)}{d\eta_0} \vartheta(\eta_0) d\eta_0 \qquad 35$$

$$\vartheta(\eta) = \lambda \int_0^\infty H(\eta, \eta_0) \sigma^2 U(\eta_0) u(\eta_0) d\eta_0. \qquad 36$$

Only the velocity profiles remain to be defined. Görtler's velocity profiles have the property that $U(\eta) = 1$ for $\eta \ge 1$ (that is for $y \ge \delta$, since $y = \eta\delta$), so the interval for the first integral equation falls on $0 \le \eta_0 \le 1$. In the second integral

equation he: limits the upper limit of integration to $\eta_0$, integrates, allows for $\eta_0 \to \infty$, and adjusts $u(\eta_0)$ to connect exponentially to the soluton. Hämerlin selects for numerical evaluation the interval $0 \leq \eta_0 \leq 1$.

The Physical Nature of $\lambda$, a theorem by Jentzsch [12, p.298]

The following steps show that the vortices can and do appear only over concave surfaces ($R > 0$),

1. Change of variables, so the integration domain in the new variables becomes [0,1],

$$\eta_0 = \frac{\zeta}{1-\zeta}, \eta = \frac{x}{1-x}. \quad 37$$

2. In the new variables the kernels take on the form:

$$\bar{G}(x,\zeta) = G\left(\frac{x}{1-x}, \frac{\zeta}{1-\zeta}\right)\frac{1}{(1-\zeta)^2} \quad 38$$

$$\bar{H}(x,\zeta) = G\left(\frac{x}{1-x}, \frac{\zeta}{1-\zeta}\right)\frac{1}{(1-\zeta)^2}. \quad 39$$

3. He changes variables once more

$$\zeta \to t \quad 40$$

$$x \to \zeta. \quad 41$$

4. He constructs a single integral by placing (35) in (36), so the information from the Navier-Stokes equations now in just one equation.

$$\bar{\vartheta}(x) = -\lambda^2 \int_0^1 \bar{H}(x,\zeta)\bar{U}(\zeta)\left(\int_0^1 \bar{G}(\zeta,t)\frac{d\bar{U}(t)}{dt}\bar{\vartheta}(t)dt\right)d\zeta. \quad 42$$

The constant in front of the outer integral sign now becomes $-\lambda^2$

5. He creates a new kernel:

$$K(x,t) = -\frac{d\bar{U}(t)}{dt}\int_0^1 \bar{H}(x,\zeta)\bar{U}(\zeta)\bar{G}(\zeta,t)d\zeta \quad 43$$

for

$$\bar{\vartheta}(x) = \lambda^2 \int_0^1 K(x,t)\bar{\vartheta}(t)dt \quad 44$$

and similarly

$$\bar{u}(x) = \lambda^2 \int_0^1 K(x,t)\bar{u}(t)dt. \quad 45$$

6. He creates new function out of Eq.

$$g(s) = \bar{u}(s) \qquad 0 \le s \le 1 \quad 46$$

$$g(s) = \bar{\vartheta}(s-1) \qquad 1 \le s \le 2 \quad 47$$

$$g(s) = \int_0^2 L(s,t)g(t)dt \quad 48$$

Where:

$$L(s,t) = -\bar{G}(s,t-1)\frac{d\bar{U}(t-1)}{dt}, \qquad 0 \le s \le 1, \qquad 1 \le t \le 2 \quad 49$$

$$L(s,t) = \bar{H}(s,t)\bar{U}(t), \qquad 0 \le t \le 1, \qquad 1 \le s \le 2. \quad 50$$

7. A theorem from Jentzsch in the theory of the Fredholm Integral Equatons of The Second Kind states that any kernel that is square integrable and becomes zero at most once, always has smallest real positive eigenvalue. [12, p.298].

Hämmerlin goes on to show that the requirements of the Jentzsch theorem are fulfilled, since: all Green's functions: $G(\eta,\eta_0), H(\eta,\eta_0)$ go to zero exponentially in the limit $(\eta_0 \to 0, \eta \to 0)$, see (31, 32, 33, 34). Similarly the velocity profile $U(\eta_0)$ and its derivative $\frac{dU(\eta_0)}{d\eta_0}$ exponentially approach zero

whithin the boundaries of the kernel $K(x,t)$: $0 < x < 1$, $0 < t < 1$. That shows that $K(x,t)$ becomes zero only once, and that is at the boundary of the interval, what is one of the main requirements of the Jentzsch theorem. The other two requirements are that the kernel $K(x,t)$ has to be positive and square integrable. He shows those requirement to be present. Then in result the theorem states that the integral equation has a smallest, real, simple eigenvallue that is smaller than all other eigenvalues. Then $\lambda^2$ (the eigenvalue of the integral equation for $g(s)$) has to be positive, simple, and real, meaning that $R$ has to be positive and the flow can only appear over a concave surface ($\lambda^2 = \mu = 2Re^2 \frac{\delta}{R} \equiv 2\text{Gö}^2$). Imaginary $\lambda$ would mean a negative radius, descriptive of a convex surface.

Note: The 2 multiplying Gö comes from RHS of (16) it is just a factor there, see also (20).

Iteration Method for Finding the Lowest Eigenvalue

The following iterations method for a system of non-adjoint integro/differential equations was proposed by H. Wielandt, [7]. Its main requirement is that for the method to give results the eigenvalues must be real and simple.

For any integral equation of the form:

$$h(x) = \varepsilon \int_0^1 M(x,t)h(t)dt$$

the series $h_v(x)$ converges. Since for the algorithm the eigenvalue is the unknown the actual calculation that takes place is of the form:

$$h_v(x) = \int_0^1 M(x,t)h_{v-1}(t)dt,$$

so that the reciprocal ratio converges uniformly to the smallest eigenvalue $\varepsilon_1$. Here since the algorithm converges uniformly, see (51), and $h_{v-1}(x) > h_v(x)$ then the initial guess for the function $h_0$ , in our case $\vartheta_0$ should be high. The ratio of of $h_{v-1}(x)$ and $h_v(x)$ for a fixed value of the independent variable converges to the smalles eigenvalue $\varepsilon_1$. In our case $\vartheta$ and $u$ are functions of the dimensionless number $\sigma$ :

$$\lim_{v\to\infty} \frac{\boldsymbol{L}h_{v-1}(x)}{\boldsymbol{L}h_v(x)} = \varepsilon_1 \qquad 51$$

where $\boldsymbol{L}$ denotes linear functional. Linear functional means that the integral maps a function into a real number [25] and here is used directly following Hämmerlin [10].

$$\frac{\boldsymbol{L}u_{v-1}(x)}{\boldsymbol{L}u_{v+1}(x)} = \frac{\boldsymbol{L}u_{v-1}(x)}{\boldsymbol{L}u_v(x)}\frac{\boldsymbol{L}u_v(x)}{\boldsymbol{L}u_{v+1}(x)} = \varepsilon^2 \qquad 52$$

$$\frac{\boldsymbol{L}\vartheta_{v-1}(x)}{\boldsymbol{L}\vartheta_{v+1}(x)} = \frac{\boldsymbol{L}\vartheta_{v-1}(x)}{\boldsymbol{L}\vartheta_v(x)}\frac{\boldsymbol{L}\vartheta_v(x)}{\boldsymbol{L}\vartheta_{v+1}(x)} = \varepsilon^2. \qquad 53$$

Since Eqs. (35, 36) are coupled, Hämmerlin starts the iteration algorithm by choosing a constant value for the function $\vartheta_o$ for initial guess of $\vartheta_o = 1$. He also chooses the straight line velocity profile: $U(\eta) = \eta$ for $0 \le \eta \le 1$, $U(\eta) = 1$ for $1 \le \eta$ . He substitutes these in (35) and gets a value for $u_1$ and uses that value in (36) and the above velocity profile to get a value for $\vartheta_2$ and so on. It is the values of $u_1, u_3, u_5$ that he uses for the ratio on the LHS of (52) and $\vartheta_0, \vartheta_2, \vartheta_4$ for the ratio on the LHS of (53). He finds curves for $\mu$ that are a function of $\sigma$ (the

other dimensionless varible Eqs. 25, 26). He also in the just like Gö makes the results for the straight line velocity profile comparable with several other velocity profiles with using equal momentum thickness, to compare the results for the lowest value of the Görtler number with similar results from other velocity profiles. Hämmerlin starts with the simplest velocity profile-the straight line. The ratios of the functionals from (52, 53):

$\frac{\boldsymbol{L\vartheta_0(x)}}{\boldsymbol{L\vartheta_2(x)}}$ , $\frac{\boldsymbol{Lu_1(x)}}{\boldsymbol{Lu_3(x)}}$, $\frac{\boldsymbol{L\vartheta_2(x)}}{\boldsymbol{L\vartheta_4(x)}}$, $\frac{\boldsymbol{Lu_3(x)}}{\boldsymbol{Lu_5(x)}}$, give values for $\lambda^2$ waht was equivalent to $\mu$.

The curves of the eigenvalues (Gö) $\equiv \sqrt{\frac{\mu_1{}^{(\nu)}}{2}}(\sigma)$ are shown in Figure 9. The index $\nu$ is the index of the numerator on the left side of Equations (52, 53).

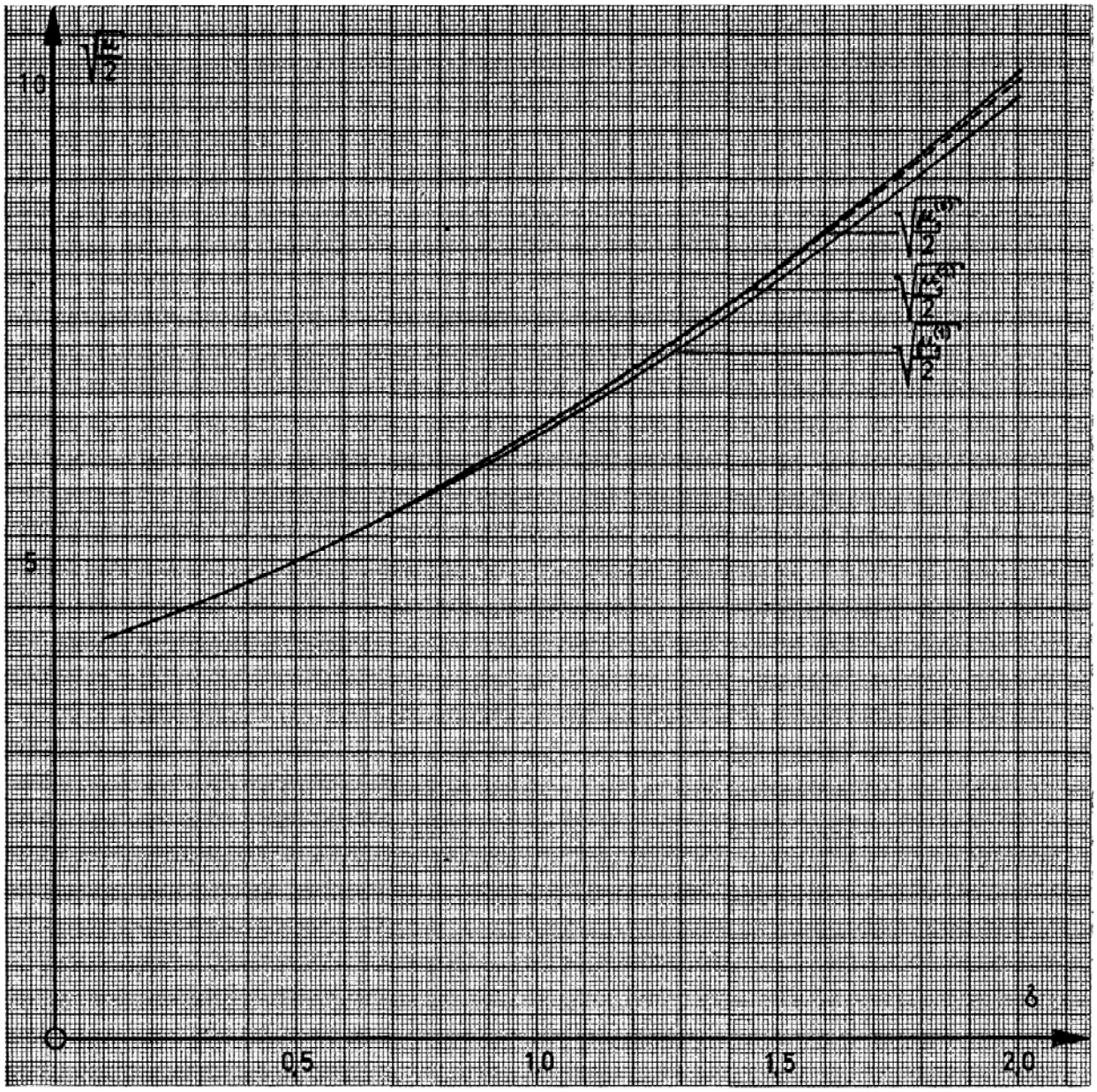


Figure 9 Graph of the results from Eqs. 43.1 for $v = 2,3,4$ for the straight line velocity profile as a function of σ [10]. $\sqrt{\frac{\mu}{2}}(\sigma)$ is the Görtler number $\sqrt{\frac{\mu}{2}} = \frac{U_0\delta}{v}\sqrt{\frac{\delta}{R}} \equiv$ Gö. For $\sigma$ see (18),(19) $\sigma = \alpha\delta = 2\pi\frac{\delta}{\lambda}$.

Figure 9 shows values that are a little lower than those of Görtler. In Hämmerlin‘s solution there is no lowest value for $\sqrt{\frac{\mu}{2}}(\sigma)$ (the Görtler number) in

the domain $\sigma > .1$ , see Figure 9.. Apparently for a flow over a slightly concave surface the vortices are present even for very low free stream velocity. The shallow flow over an axially infinite concave surface is very similar to the shallow flow in an axially infinite rotating cylinder.

Conclusion

Hämmerlin succeeded in showing that the vortices exist for very small values of Gö, Figure 9. Solving the Navier-Stokes equations for the existence of the vortices requires knowledge in solving a system of two non-adjoint integral eigenvalue equations. A method for solving those was first published by Helmut Wielandt in 1944 [7]. To understand this iterative method one needs an example and Hämmerlin provides one by applying the method to the fully developed Görtler vortices.

# 2. METHODS

Discussion

The apparatus for studying the flow consists of:

- digital video camera: SONY DCR-SR200
- Laser Photo/Contact Tachometer, Extech Instruments- to measure the rotation rate of our cylinder.
- Red food dye color for the water

We experienced a lot of turbulence from the lower viscosity. The lower surface tension though helped with bubble incorporation and vortex visualization. Balmer [2] used SAE motor oil with dynamic viscosity of ≈ 150 cP, and Thoroddsen [14] used liquids of ≈10-1000 cP, a lot higher than our distilled water at ≈1 cP. Increasing the dynamic viscosity, lowers the Görtler number. We observed a more non-uniform, less defined flow front due to our much lower dynamic viscosity and higher tangential speeds. Our rotation rates, of up to 1400 RPM were 3-4 times higher than those used by Thoroddsen [14]. The ability of our cylinder to spin more than two gallons of water made it indispensible in studying the gravitational effects of liquid over the Boundary layer. Since the vertical gravitational push of the suspended pool of water on the boundary layer can be compared to the normal centrifugal push of water on the boundary layer in a curved duct, the study of the vortices in a rotating cylinder increases in importance.

In the stage before bubble formation the vortices become evident by surface waves and a wavy pattern of the flow front along the $z$ – axes Figure 33, Figure 34. In chapter 3 it is shown that that pattern is a result of a Coriolis force.

Benefits from the lower viscosity, higher rotation rates, and higher fill volume fractions include: higher Görtler number, stronger vortices, better visualization. Bubbles caught in the vortices are easier to track at high speeds, by making almost continuous flow lines, allowed for great slow motion recording. An attempt to visualize the vortices with pellets failed with the pellets severely scratching the inside of the cylinder even at low tangential speeds.

The viscous interference of the suspended over the boundary layer pool of water with the Coriolis effects of the vortices increases with increase of the fill-volume. So the pool of water indirectly places a brake on the vortices.

Apparatus

The apparatus for generating the flows in a rotating cylinder consists of

a) The supporting frame

It is precision aligned and milled from aluminum bars that have a right triangle profile. We used 1" wide rollers for support of the cylinder, see Figure 10 through Figure 23.

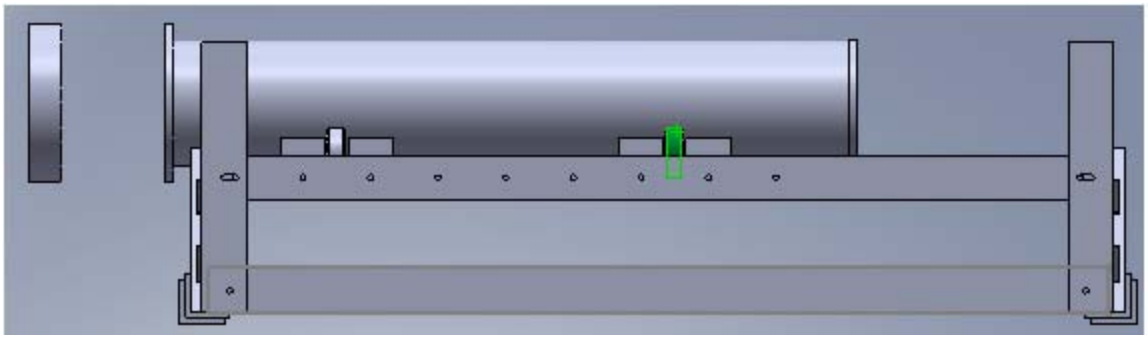

Figure 10. Left view of supporting frame and cylinder

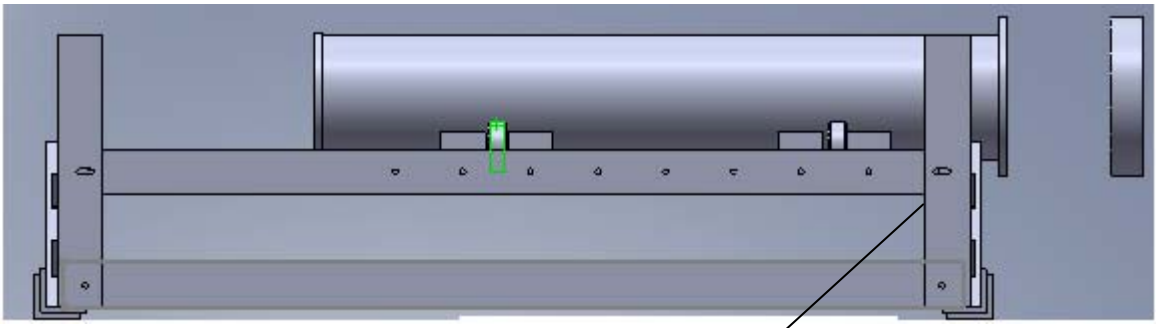

Figure 11. Right symmetrical view of supporting frame and cylinder

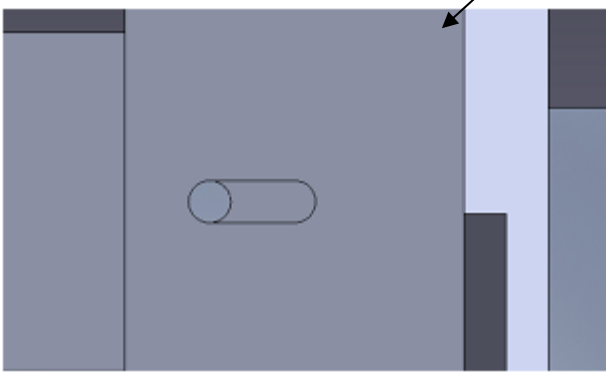

Figure 12. Detail of groove and hole. Such fastening allows for the horizontal bar to fit flush against the inside of the vertical bar

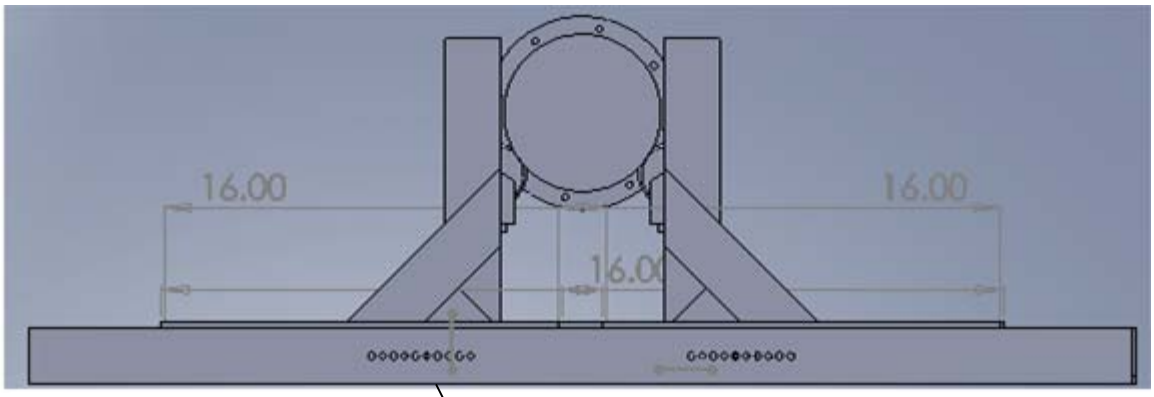


Figure 13. Front view of cylinder and the supporting frame

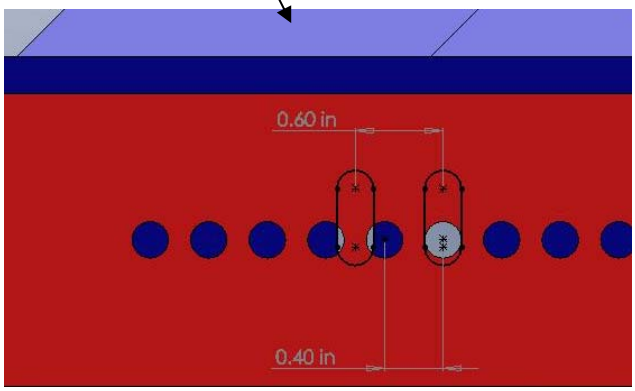


Figure 14. Groove and hole allows vertical flush fit and utilizes the concept from the Vernier caliper with the smallest increment for hole and groove alingment of .2".

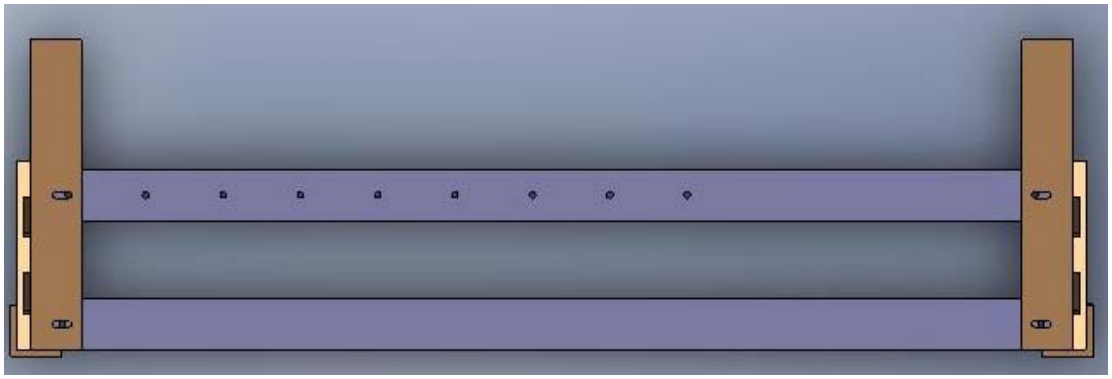

Figure 15. Sliding assembly

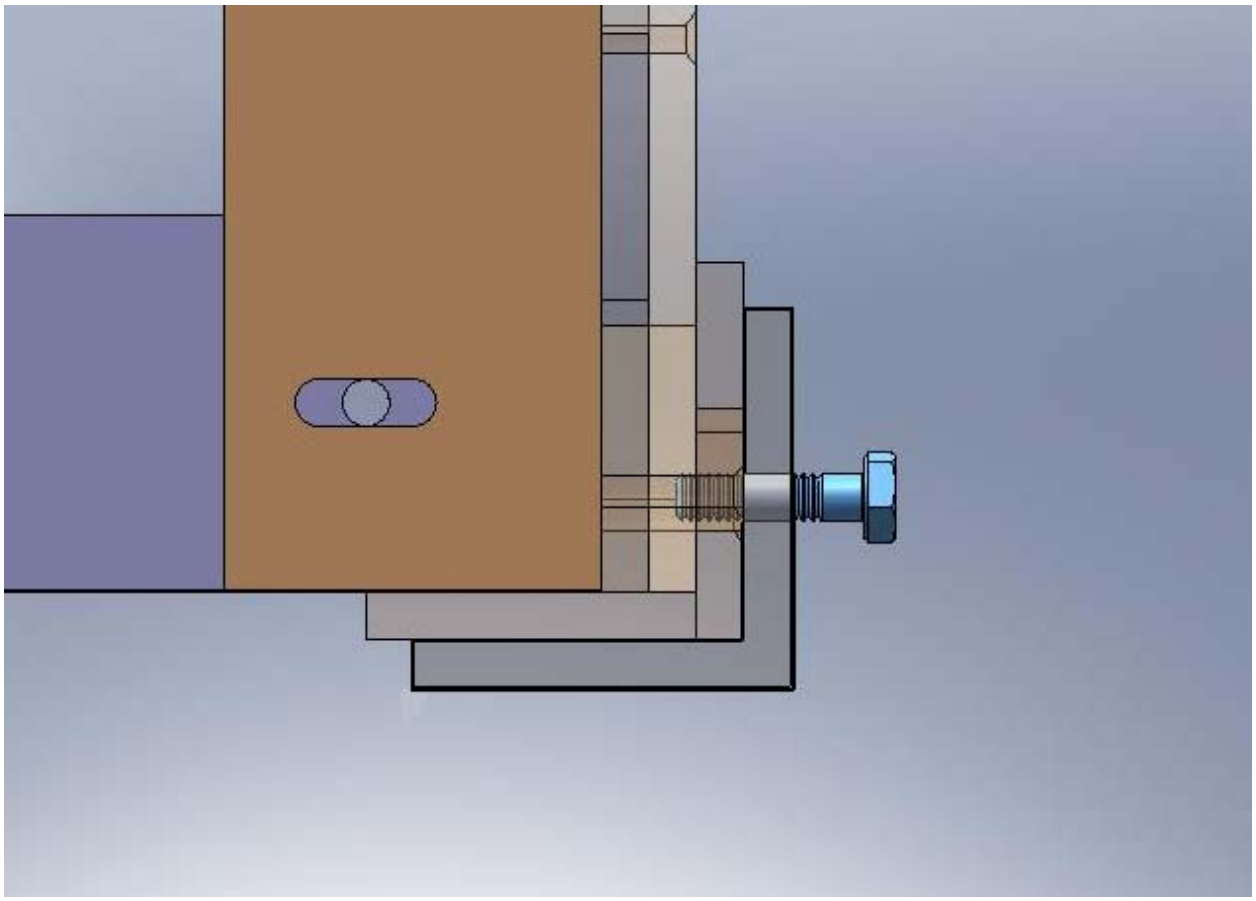

Figure 16 View of one of the ends of the sliding assembly attached with a bolt to the fixed rail. The fixed rail has the thicker border

The groove and hole method allows precise incremental horizontal alignment for the sliding assemblies. The groove and hole slider connections prevent lateral misalignment, it lowers the 2 degrees of freedom for translational motion in a plane to only 1. The distance between the two vertical grooves was inspired by the Vernier caliper and set so the connected frame can slide by incremets of half the distance between the round holes.

b) Acrylic cylinder

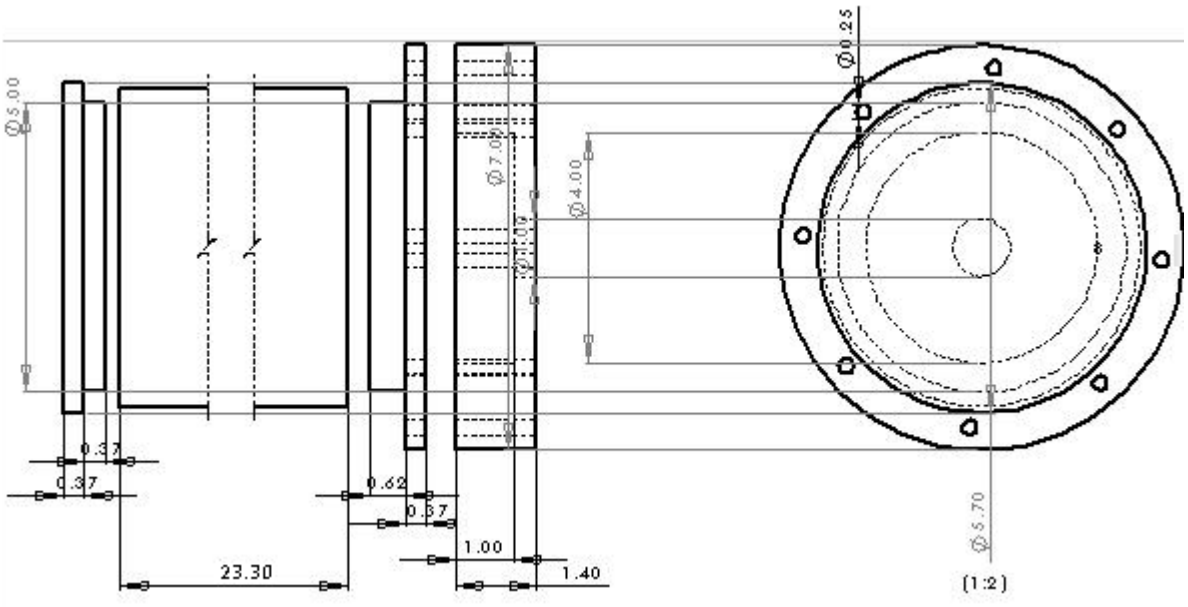


Figure 17 From left to right: lid away from motor, cylinder, lid toward the motor, and the lid that fits over the pulley and bolts to the cylinder lid that is toward the motor, all units in (in.)

The lids were built by gluing .37” and .25” thick acrylic. The lids are milled to 1/1000-th of an inch precision on a Roland MDX-650 3-D milling machine. They fit tight and are held in place by a radial frictional force between the lid and the cylinder. For the higher volume-fill fractions exist sleeves, with up to 1" radial width and .37” thickness. The sleeves fit radially outward from the ends of the cylinder and clamp the cylinder tighter against the end lids. Applying to the contact area high viscosity Dow Corning High Vacuum Grease, creates a water tight seal in the micro gaps between the two lids and the cylinder.

c) Stand for the motor

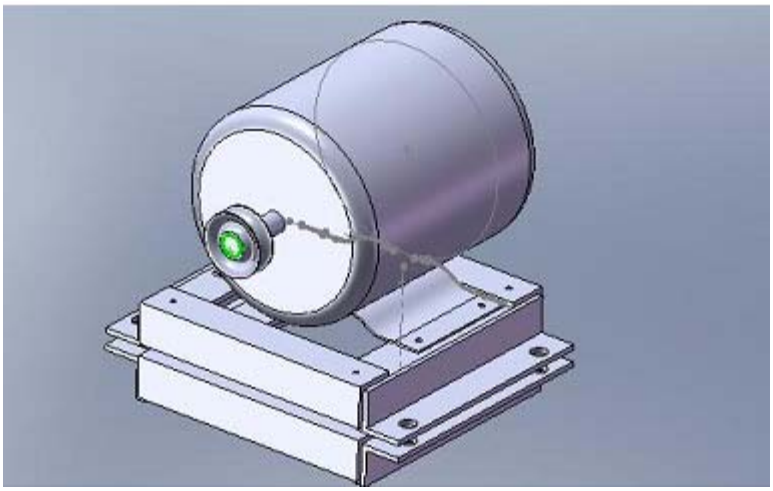

Figure 18. Motor and its base

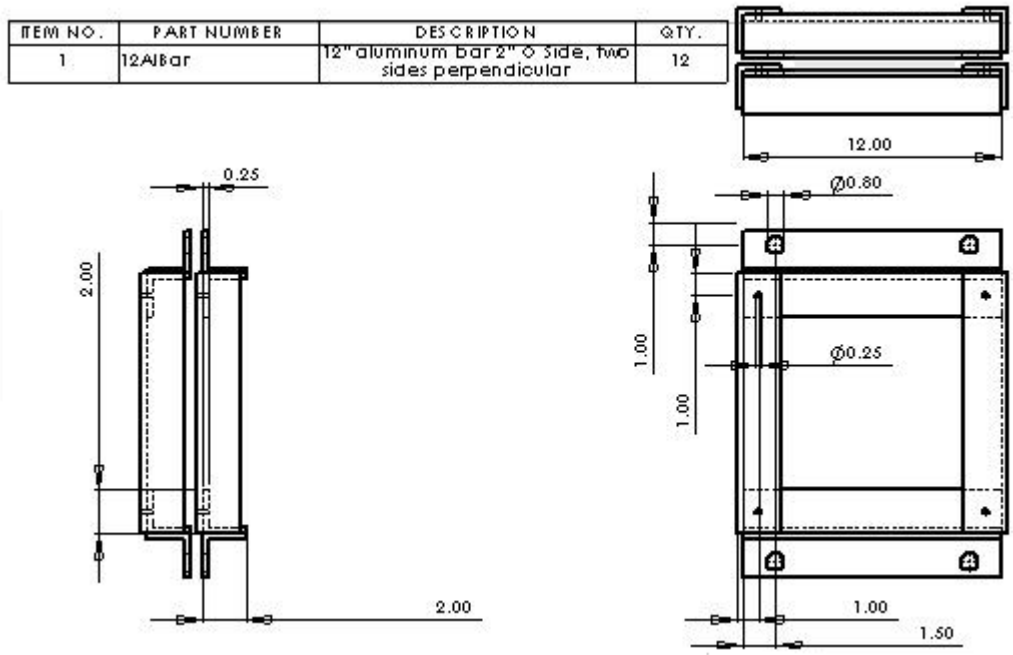


Figure 19. Adjustable base for the motor, all units in (in.)

The base for the motor is shown in Figure 19. The elevation of the four corners is adjusted through bolts that fit through the Ø.8″ holes. This method of

support allows us to change the azimuth and zenith orientation of the motor axle. If all four big bolts are turned simultaneously that changes the distance from the motor axle to the table.

We solved the alignment problems by adding a lid to fit over the pulley of the motor on the side between the pulley and the motor, Figure 10, Figure 11, Figure 20, and Figure 22. The lid between the pulley and the motor can be improved with increasing its outer radius and being built on a 3-d printer.

Total Apparatus

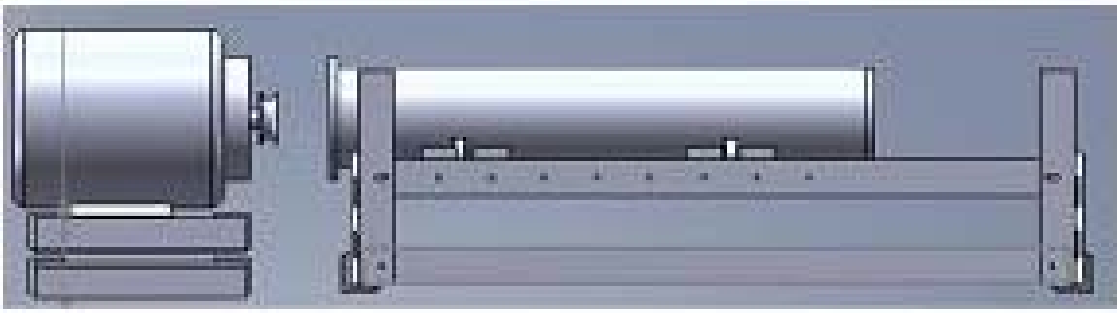

Figure 20. Complete apparatus, side view,

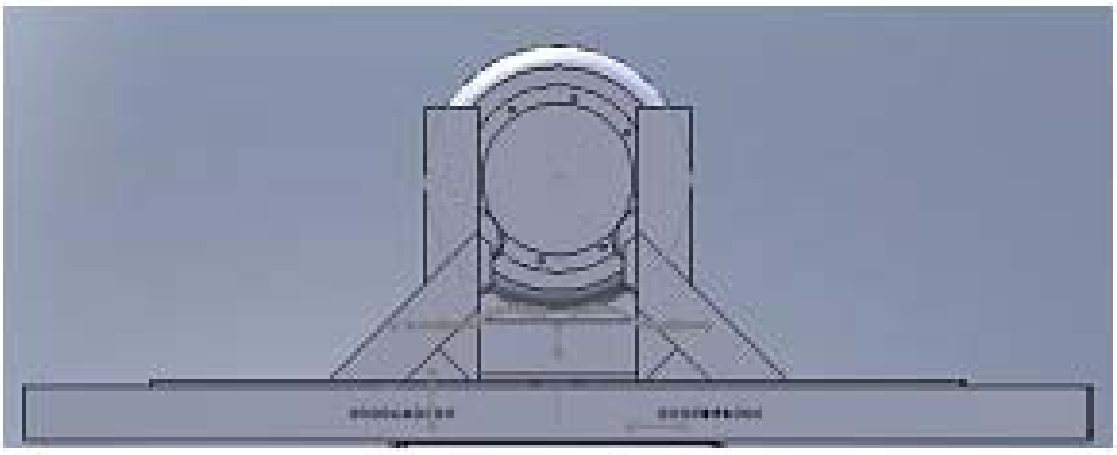

Figure 21. The complete apparatus, view opposite from the motor

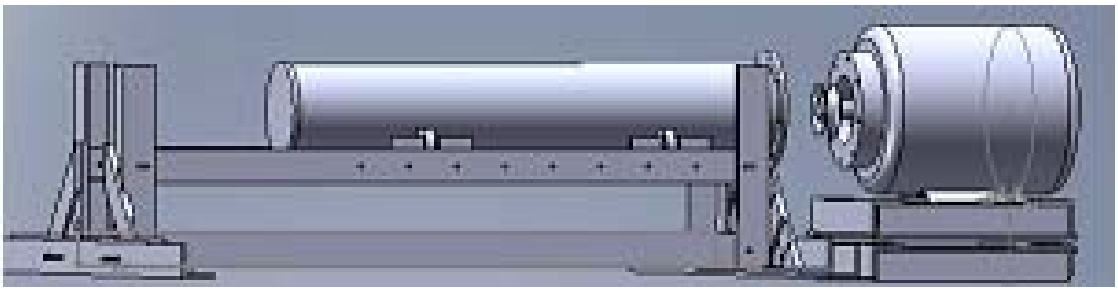

Figure 22. Angled side view, of the sliding assemblies, fixed rails, motor, motor frame, cylinder, and lids.

Advantages of the Apparatus:

- Ability to accept cylinders with big radius and more importantly with big volume, up to 7500 mL.
- Ease of alignment of cylinder and motor
- The direct drive eliminates friction losses and damage of transmission or belt. It allowed us to reach very high rotation speeds, up to 15 m/s tangential speed. The pulsed starts of the motor would have damaged any transmission.

# 3. FINDINGS

Papers on the topic “Fluid in a rotating cylinder” focus on naming different flows resulting from the Görtler vortices or from the motion of the enveloping the vortices boundary layer: like Hygrocyst [2] , Shark teeth, ribbing flow, pendant waves, [5,6]. Many authors do not even mention the Görtler vortices. They missed the opportunity of studying the properties of the underlying engine of all meaningful flow patterns in a rotating cylinder. The vortices are related to the Taylor vortices (Figure 1, Figure 2, Figure 3, and Figure 4) with differences in the way the gravitational force affects the flow and the limiting factors on the growth of the boundary layer. For the Taylor vortices the maximum diameter of the vortices is limited by the distance between the inner and the outer cylinders. For Görtler vortices in a horizontally rotating cylinder the limit, if there is enough water, is the diameter of the cylinder. The size of the vortices is a function, see Görtler number, of the free-stream velocity, defined to be the velocity difference between liquid at the lowest and the highest radial points of the boundary layer. The vortices are periodic for any tangential speed of rotation only in a semi-infinite cylinder, one that is infinite in the axial direction. In a finite cylinder is impossible to fit an integer number of wavelengths for each value of the tangential speed, since the wavelength is a function of the free-stream velocity. In the length of the cylinder we have observed that for all diameter cylinders and for any liquid fill fraction there is a discrete set of tangential speeds of the inner edge of the

cylinder which form axially stable down-wash regions. They do not fluctuate along the symmetry axes of the cylinder. Only at specific small intervals in the tangential speed of the inner edge can vortex wavelengths be definitively measured for a finite cylinder. The wavelength is the most important variable since it determines the location of the important down-wash regions. Hämmerlin's paper gives the most insight into the boundary conditions that might be a result of his discussions with Görtler what other contemporary papers on the topic lack, [16].

Flow over a concave surface is similar to the flow in a rotating cylinder. In the first, liquid moves over a surface, and in the second the surface moves from under the liquid. The advantage of the rotating cylinder is the localizing in space of the flow front. Günter Hämmerlin already showed for a concave surface that the vortices exist even for negligible free-stream velocity. One of Hämmerlin's assumptions, the fixed wavelength, is only valid for the axially-infinite cylinder. The hypothesis is that for every fill-volume fraction exists a discrete set of speeds each member of the set corresponding to an axially stable down-wash regions and therefore to an even number of vortices that have a fixed in space axial position.

Unlike for the Taylor case in the case of the horizontal cylinder air bubbles start incorporating in the flow so that the kinematic viscosity ($v$) increases making the flow more compressible, $\text{Gö} = \frac{U_0 \delta}{v}\sqrt{\frac{\delta}{R}}$ decrases and the average wavelength slightly decreases, Figure 5. It is apparent that slight

imprecision will prevent the manifestation of the stable Hygrocysts/down-wash regions. The imprecisions for us come from nonuniform wall thickness of the Plexiglas cylinders. The supporting rollers do not stay rigid but deform during the rotation.

Our apparatus is superior to any other that I have seen in its range of operating speeds and weight of the enclosed liquid. It allows for the spin of 8789 mL of water at up to 800 RPM in a 7" ID cylinder, or 1900 mL at 1500 RPM in a 3" ID cylinder. Small imperfections in cylinders with small radius can add to obstructive centrifugal forces like in the case of our 3" cylinder. We only used long cylinders since short ones will allow for very few down-washes to form. An important consequence of recording the distance between axially stable down-wash regions is that it is also a measure of the boundary layer thickness-BLT, namely the BLT is equal to half a wavelength, Figure 5.

The wavelength increases with increase in the water volume and the tangential speed. For example here is a list of the maximum down-washes in the 9/10 fill before forming solid body:

- in the 3" cylinder form 6 Hygrocysts,
- in the 5" cylinder form 3 Hygrocysts,
- in the 7" cylinder form 2 Hygrocysts,

The vortices have a cylindrical symmetry that can grow in diameter up to the diameter of the cylinder. So for the 3" cylinder the 6 Hygrocysts stand for 12 vortices. In conclusion to have comparable data for similar RPM for different

diameter cylinders, the cylinders should have the same aspect ratio $\left(AR = \frac{L}{D}\ [23]\right)$.

The higher aspect ratio of the 3.012" cylinder allows it to contain more vortices than the 5" or 7" cylinders, Figure 26. While in the 5" and 7" cylinders the vortices could become axially fixed, for the 3" cylinder the vortices were too weak to observe the phenomenon of axially fixed vortices. The Görtler number increases with decreasing the radius of curvature, but the important thing here is not curvature but the square root of the centrifugal acceleration that hides in the Görtler number. That acceleration is low for the 3" cylinder, and is highest for the 7" cylinder, and that determines the width of the intervals in the domain of tangential speeds where the vortices become axially stable. The intervals in the RPM domain at which the down-wash regions become axially stable is narrower for the 3" cylinder.

Additional problems that prevented us from observing stable down-wash regions came from the inner and outer edges of the 3.012" cylinder not being concentric, Figure 23.

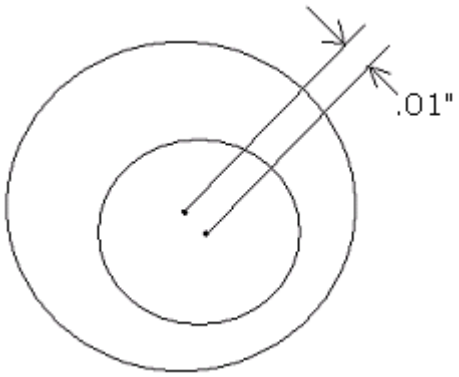


Figure 23 Difference in concentricity of inner and outer edge for the 3" cylinder

This imprecision added a small centrifugal instability that lead to a vibration that may have affected the axial stability intervals in the RPM domain.

For the existence of Görtler vortices in a rotating axially infinite cylinder Bottaro and Abdelfattah solved the Navier-Stokes equations with the continuity equation, and similarly to the flow over a semi-infinite concave surface they calculated that the vortices are present even for very low tangential speed of cylinder rotation [10,24]. This thesis is an extension to the theoretical work of Hämmerlin and Görtler where the fixed wavelength was one of their solving assumptions. Here the question is what if the wavelength varies like is the case for varying boundary layer thickness that results from changing the free stream velocity. The vortices' wavelength is a measure of their individual strength. This paper proposes the existence of a discrete set of speeds of rotation, that represent axially stable vortices. The theoretical notion of a fixed wavelength for a flow over an axially-infinite concave surface does not automatically translate to finite horizontally-rotating cylinders.

For the horizontally-rotating cylinder the axial boundaries introduce the Gibbs phenomenon, the notion of the fixed wavelength for axially infinite cylinder is substituted with the notion of axially stable vortices, for an axially finite cylinder. The Gibbs phenomenon present in rotating finite cylinders manifests itself through stronger vortices close to the axial walls Figure 26. The gravitational effects from the pool of water suspended over the boundary layer largely influence the flow in cylinders of varying curvature and 7/10, 8/10 and 9/10 fill-volume, see the section on it on pg. 45.

Gibbs Phenomenon in a Rotating Cylinder

The Gibbs phenomenon appears when expanding discontinuous functions in Fourier series. The Fourier series approximation of the rectangular function takes on an integer number of peaks within the domain of the rectangular function.

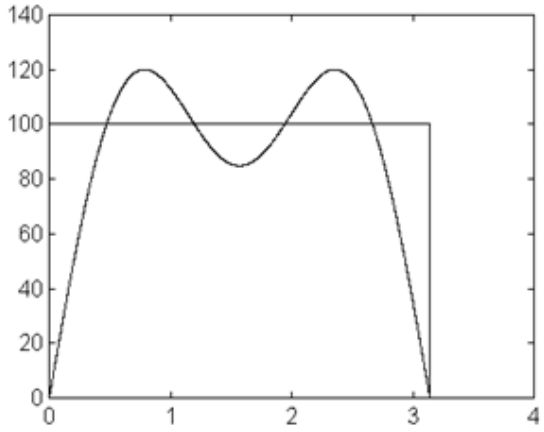


Figure 24. Gibbs phenomenon 2 terms [19]

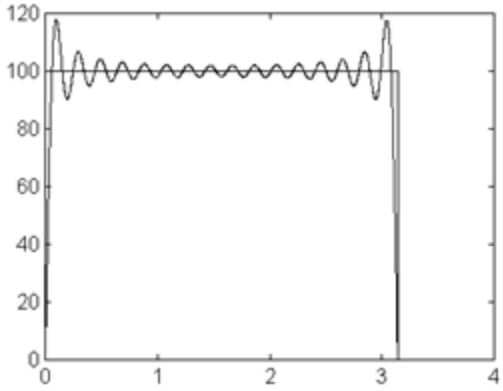


Figure 25. Gibbs phenomenon 16 terms (note the 16 half wavelengths) [19]

The rectangular function expanded in *sin* and *cos* terms by the Fourier series approximates on a closed interval a function that is not differentiable at everywhere in the interval (nonsmooth function) with an everywhere infinitely differentiable smooth wave function. If we named the distance between two neighboring local maxima half a wavelength, the Fourier transform approximates the rectangular function with an integer number of half wavelengths (terms) Figure 24, Figure 25. The partially filled cylinder, even if it were semi-infinite, has axial boundaries and within them for a random value for the RPM the vortex wavelength takes on a value from the set of real numbers. The Gibbs phenomenon manifests through fractionally stronger vortices at the axial ends, evidenced by a longer wavelength Figure 26.

Figure 26 End view of the Gibbs phenomenon in a cylinder with an aspect ratio of ~10, 5/10 fill-volume, (extracted from video).

In the cylinder just like in the case for the Fourier series expansion of the rectangular function there are two boundaries that limit a one-dimensional (axial) domain of the vortices. It is the vortices that do the Fourier transform of the cylinder since they are unit entities that can take on an integer number of wavelengths within the axial walls of the cylinder (for certain intervals in the continuous set of tangential speeds). That Fourier wave function has an integer number of local extrema. At the ends of the interval the Fourier series *overshoots* . An analog to the *overshoot* from analysis are the fractionally stronger vortices toward the ends that lift more water than the ones closer to the center.

Other natural systems where the Gibbs phenomenon is present are: It is the source of the 9% overshoot at the discontinuity of a square wave signal fed into an amplifier [pg.53, 21] The beam in cathode ray tubes if is made to rapidly reverse direction, like if it is traveling from left to right and is suddenly reversed back toward the left then the overshoot can cause problems [pg.53, 21]. The Gibbs phenomenon causes artifacts in spinal MRI imaging that can even lead to the (false visual) appearance of syringomyelia [22].

Centripetal Acceleration Effects on the Axial Stability of the Vortices

Contributing to the stability of the vortices could be the centripetal acceleration. We kept the dynamic viscosity constant at 1cp. Since the square root of the centripetal acceleration ($\frac{U_0}{\sqrt{R}}$) is part of the Görtler number, and in light of our observation of the complete instability for the flows of various fill-fractions in the 3" cylinder (the one with the highest curvature) we can conclude that the higher the centripetal acceleration, the higher the Görtler number, the stronger the vortices yet wider the RPM intervals where they are stable. Maybe this is why other researchers have not found the existence of axially stable vortices, since they were interested in studying smaller diameter cylinders with low fill-volume, spinning at low RPM. They used much higher dynamic viscosities [14,2], which diminishes the vortex strength. The intervals in the RPM domain where the Hygrocysts are stable are small, and easy to miss if ($\frac{U_0}{\sqrt{R}}$) is low and one is not looking for them. For the 3" cylinders they are too small and must be searched for with a digital tachometer. For a fixed kinematic viscosity, it is the square root of the centripetal acceleration ($\frac{U_0}{\sqrt{R}}$), that is in the Gö, is in general the most frequently varying parameter defining the strength of the vortices.

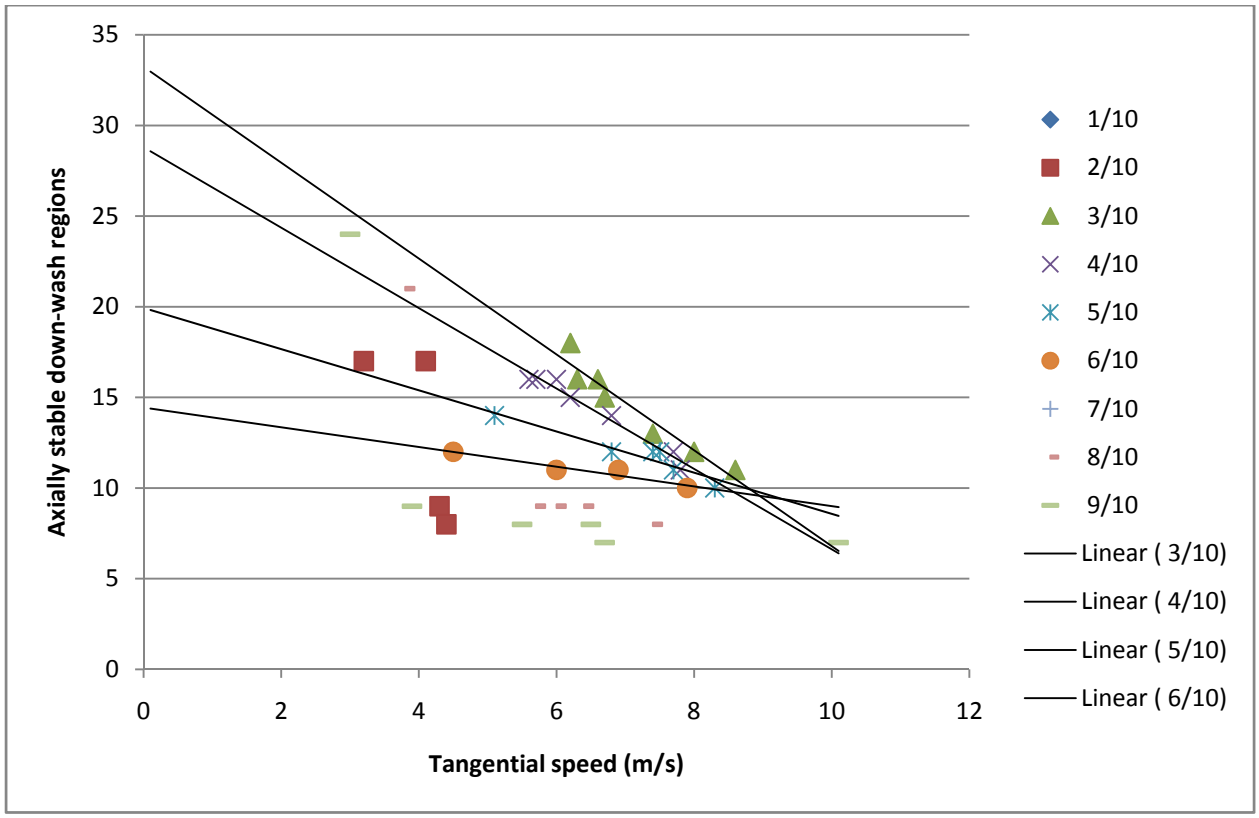


Figure 27 Line-fit for various fill-volumes for a 3" cylinder not affected by the gravitational effects of the pool of water over the boundary layer

Figure 27 recommends a starting point, in the domain of tangential speeds for a 3" cylinder of random fill-volume between 3/10 and 6/10, for easy search of axially stable vortices. That speed is approximately 8.7 m/s.

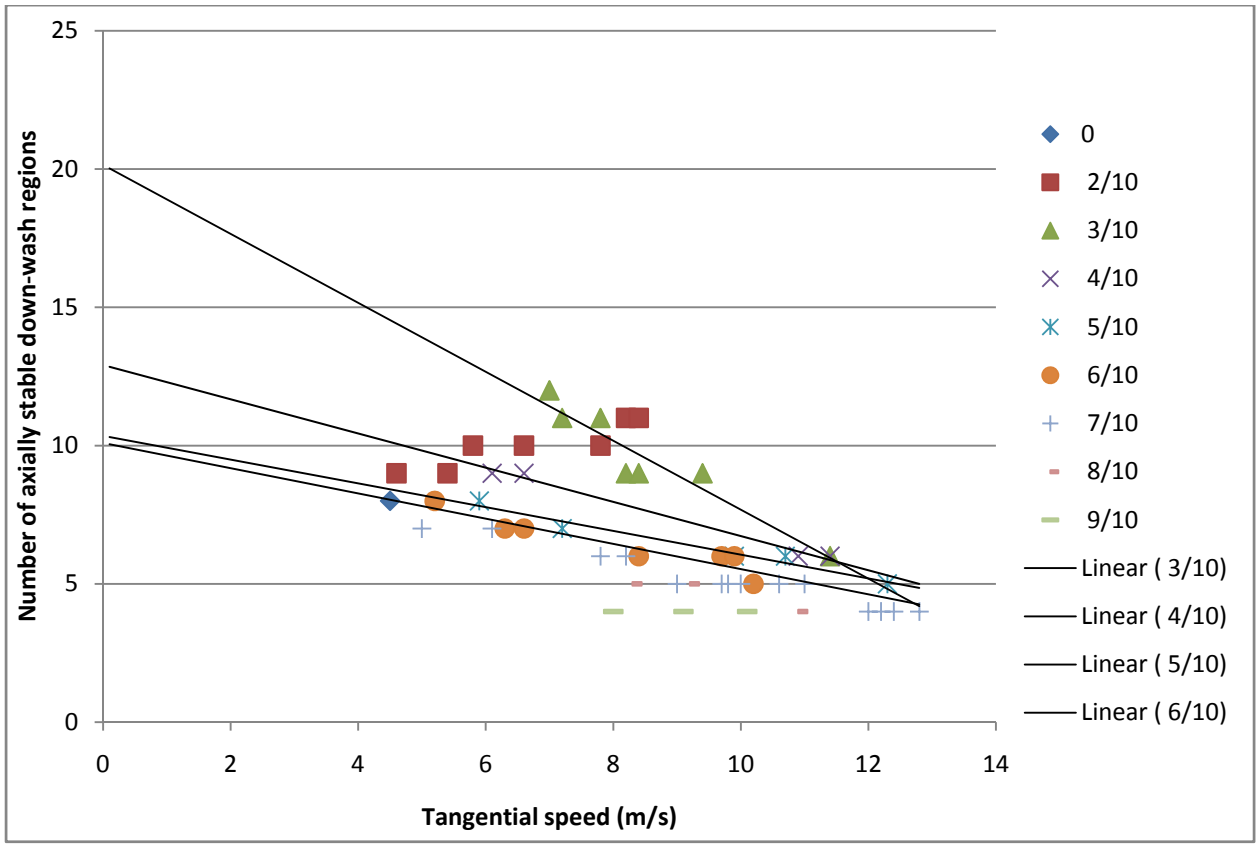


Figure 28 Line-fit for various fill-volumes for a 5” cylinder not affected by the gravitational effects of the pool of water over the boundary layer

Figure 28 similarly to Figure 27 shows a beginning point, for search for axially stable vortices for a 5” cylinder of random fill-volume between 3/10 and 6/10, at around 12 m/s.

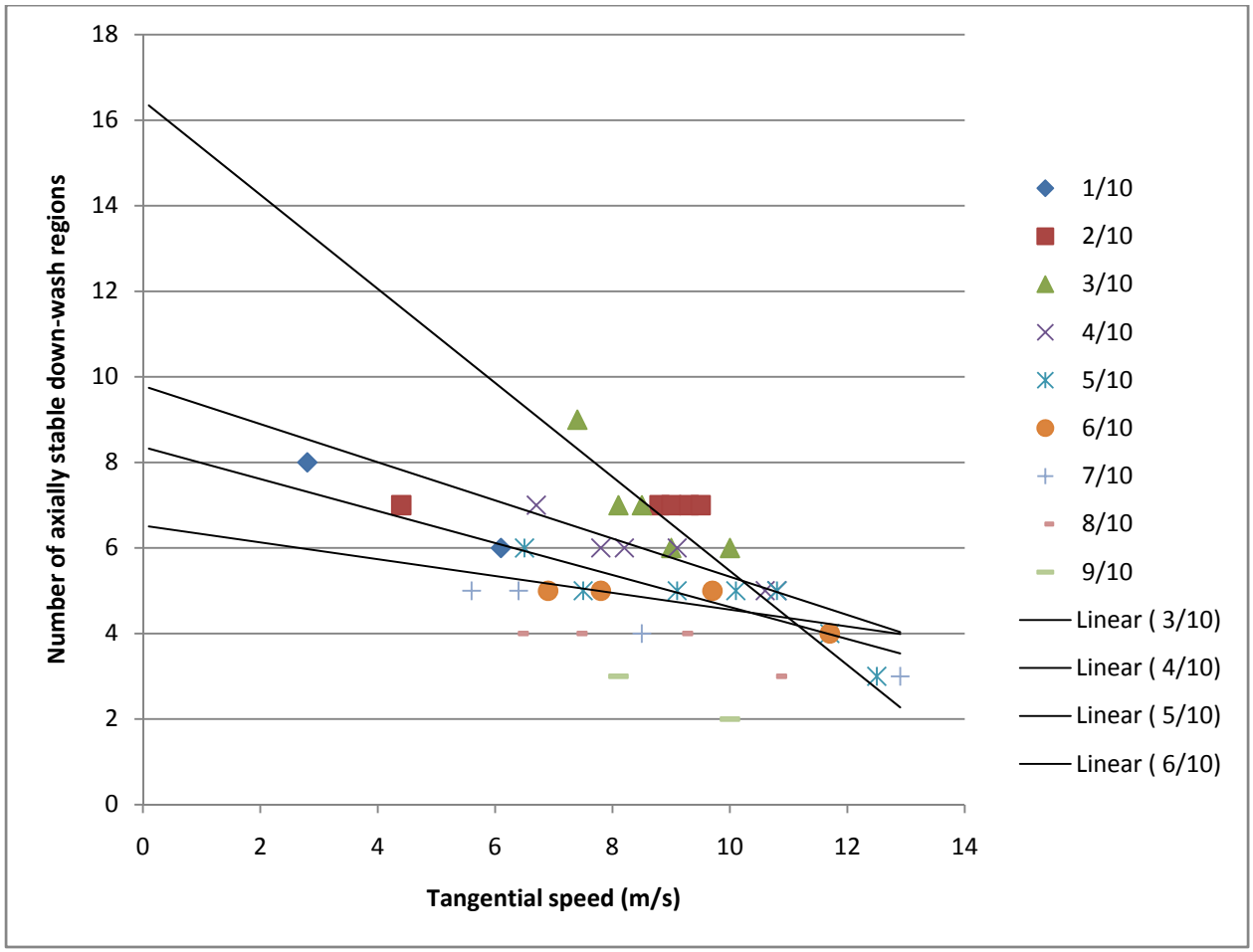


Figure 29 Line-fit for various fill-volumes for a 7" cylinder not affected by the gravitational effects of the pool of water over the boundary layer

Figure 27, Figure 28, and Figure 29 show stability regions for the various fill-volume fractions not affected by the gravitational push from the suspended pool of water over the boundary layer. The pool's gravitational interference with the vortices is much more evident for the 7/10, 8/10 and 9/10 fill-volume fractions. These stability regions occur: for the 3" cylinder at 8.7 m/s, for the 5" cylinder at 12 m/s, and for the 7" cylinder at 11m/s . So, to observe axially stable vortices for a random volume fill between 3/10 and 6/10 for a 5" cylinder one will need to spin it at around 12 m/s (900 RPM).

Gravitational Interference by the Suspended Pool Water With the Boundary Layer

An interesting phenomenon appears for the, 7/10, 8/10 and 9/10 fill cylinder where it becomes evident the growth of the vortices up until the point where the gravitational force of the suspended over the boundary layer liquid is the highest. Past that point the vortices disappear. With increased fill-volume fraction, the gravitational force by the suspended water pool on the boundary layer increases. That pool adversely affects the strength of the vortices. It increases the viscous drag and hinders the tangential shift between down- and up-wash regions. That shift is a result of the coriolis force acting on the down- and up-wash regions, see the section 'Coriolis Effects Determine the Shape of the Flow Front' . For this reason in the 7/10, 8/10 and 9/10 fill-volume the vortices exist only up until the point in the interior of the cylinder where the gravitational force is the greatest. The jets of water that still come up from the rising side of the cylinder at the points of down-wash are results of inertial effects and do not possess any trace of vorticity in them like for the 3/10 to 6/10 fill-volume fractions.

This effect is more pronounced for heavier water pools suspended over the boundary layer Figure 30, Figure 31, Figure 32. This effect is unique to a rotating cylinder since in a deep flow over a curved surface or in a flow through a curved duct the velocity difference between liquid at the top and bottom of the boundary layer is constant. For the case of a horizontally rotating cylinder

the suspended pool of water starts to rotate in the same direction as the cylinder dragged by the viscous pull of the boundary layer.

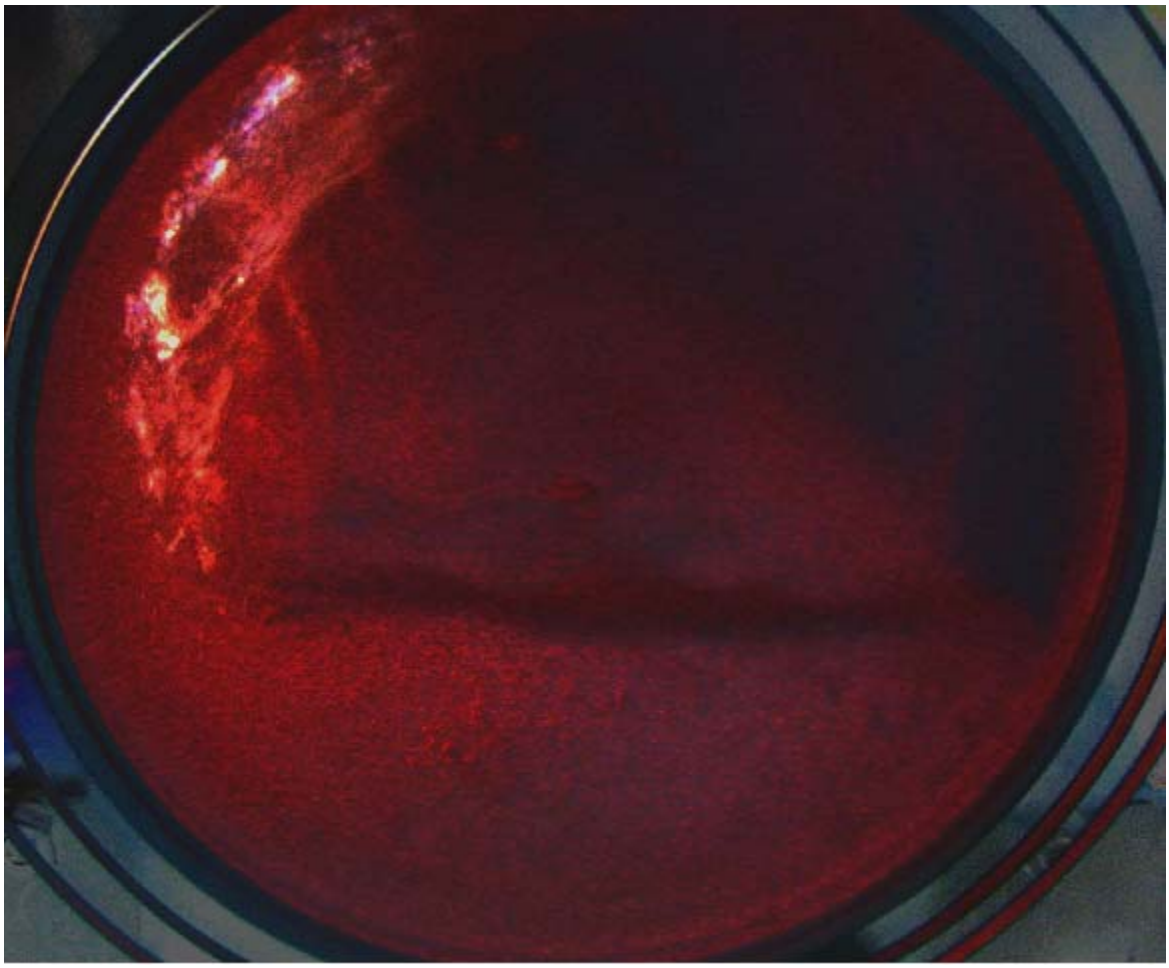

Figure 30. Picture of a small pool of water standing over the boundary layer (7", 4/10, 444 RPM). The angular velocity is into the picture. The boundary layer is visualized by the water at the rising end of the cylinder. The color scheme of the picture has been altered to improve visibility.

Note the high bubble density in fig. 34. The main difference with Figure 31 and Figure 32 is the pool of water over the boundary layer that is also dragged into rotation by the boundary layer.

Figure 31. The standing pool of water over the narrow boundary layer, 7" cyl. 7/10 full, 320 RPM, (the picture is extracted from a video). The angular velocity is into the picture. The color scheme of the picture has been altered to improve visibility.

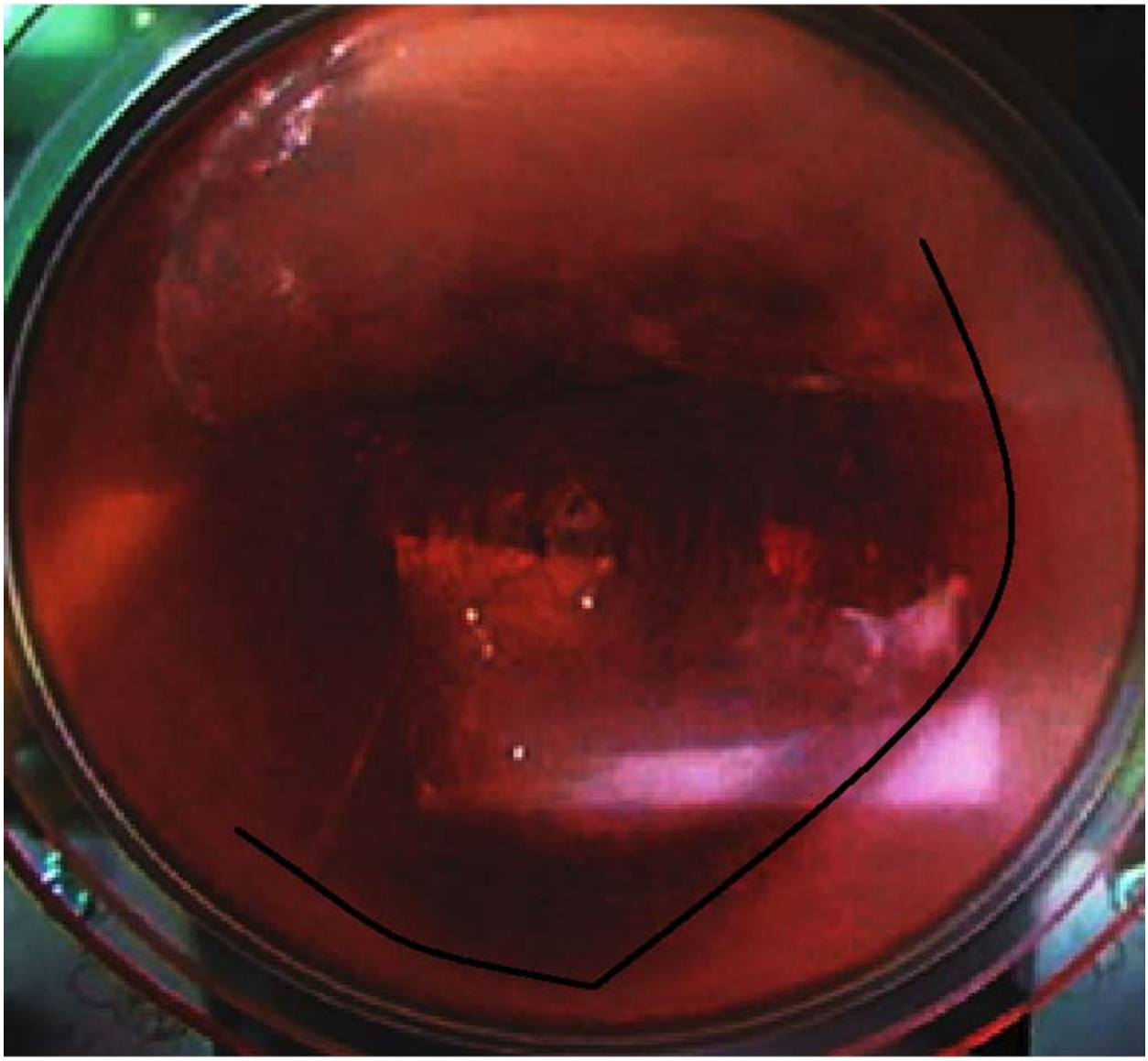

Figure 32. The standing pool of water over the narrow boundary layer , 7" cyl., 7/10 full, 303 RPM. The angular velocity is into the picture. The color scheme of the picture has been altered to improve visibility.

Notice how the bright spot on the bottom right of Figure 32 ends almost completely at the lowest point of the cylinder. Its lighter color is from the suspended bubbles. Once they are gone and the liquid becomes darker. The weight of the liquid not only pushes the bubbles out of the boundary layer, it also, places a viscous break on the coriolis effects of the vortices. Evidence of

that is the lack of vorticity in the small, periodic, by momentum driven lumps of water that pop up on the rising inner wall.

Coriolis Effects Determine the Shape of the Flow Front

Knowing the fixed locations on the z-axes of the vortices is helpful in using localized methods for heat exchange, like placing fins there whose length and shape will depend on the kinematic viscosity of the fluid that will surround the cylinder. The immense amount of bubbles that start to incorporate in the water with increasing the strength of the vortices increase many fold the water to air surface in the cylinder making it possible to create an evaporative heat exchanger. Again in this case the cylinder will have fins that optimize the heat exchange at each down-wash region.

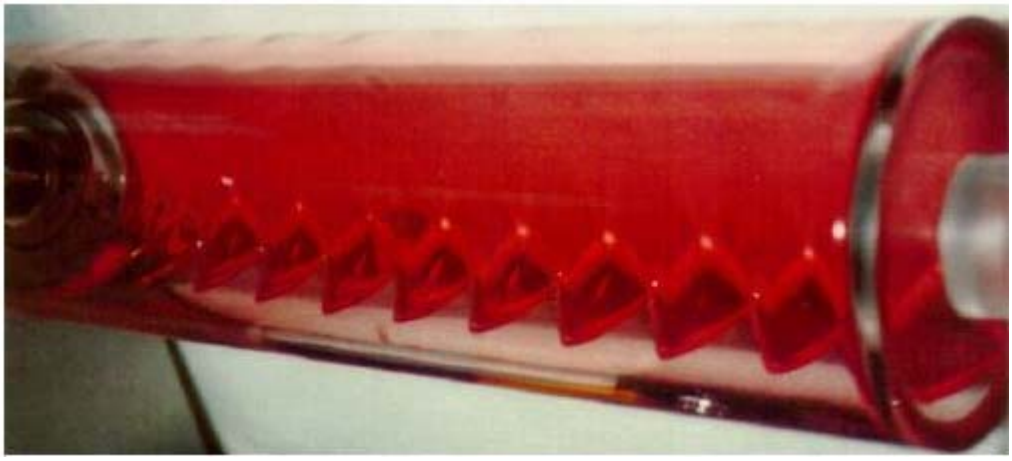

Figure 33. Shark teeth, high dynamic viscosity, rotating at 3.2 rpm, dynamic viscosity $\mu = 49$ cp, fill-fraction 6% [14]

The following figure shows a picture of the same surface effects by the vortices for much lower viscosity.

Figure 34. Picture of the surface formed at low rotational rates and low water volume fraction (7", 417 RPM). The color scheme of the picture has been altered to improve visibility.

Notice how Thoroddsen's vortices are radially bigger, Figure 33. That is from the higher dynamic viscosity of their liquid: 8 to 1030cP. In comparison our distilled water has a dynamic viscosity of 1 cP , Figure 34 [18]. The liquid that the vortices shoot up in the up-wash regions is slow in flowing down so it concentrates so well in periodic lumps at the down-wash regions. The Coriolis force cannot be ignored since the down- and up- wash flows are at right angles with the angular velocity of the cylinder. At the down-wash regions the Hygrocysts originate (Figure 8), and also the regions at the front of

Thoroddsen's "shark teeth" , Figure 33, Figure 34. The following expression is the Coriolis acceleration:

$$\boldsymbol{a}_{coriolis} = 2\boldsymbol{v}_{down(up)-wash}\boldsymbol{w}_{cylinder}.$$

It explains the different tangential velocity profiles for down-, up-wash regions, Figure 7. The orthogonality of the vectors and the factor of two make the Coriolis force a considerable force causing a tangential shift between the down- and up-wash regions. It explains how the gravitational force of the suspended pool of water over the boundary layer hinders the propagation of the vortices past lowest point in the cylinder, typical for 8/10 or 9/10 fill-volume.

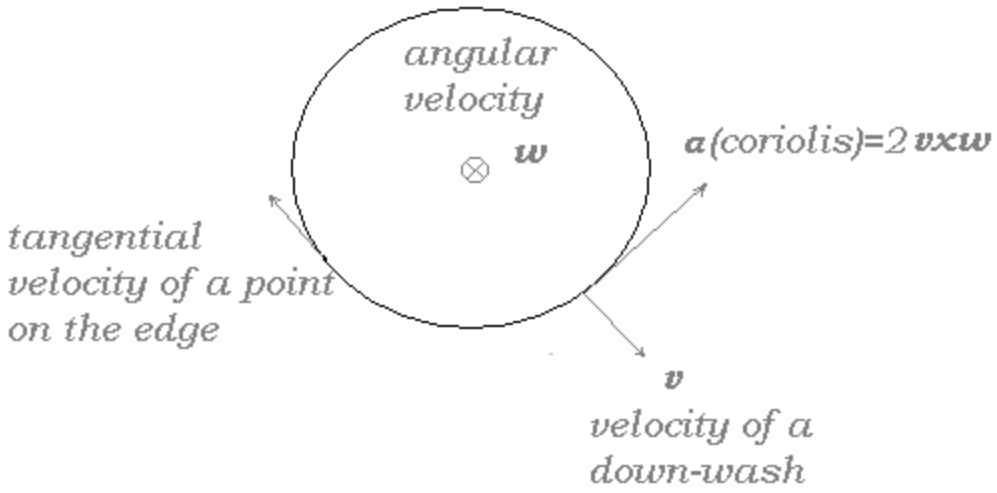


Figure 35. The Coriolis force pushes the down-wash regions in direction opposite of the tangential velocity (upstream)

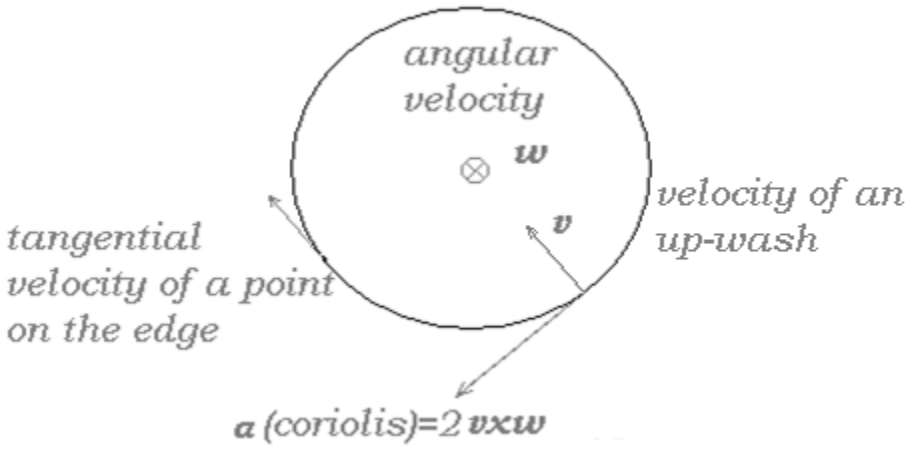


Figure 36. The Coriolis force pulls the up-wash regions downstream

From Hämmerlin's exact solution to the eigenvalue problem for the onset of Görtler vortices, it is known that the vortices exist for small values of the Görtler number, Figure 9. As a result the above observation is simply a manifestation of the Görtler vortices. The vortices' single condition for existence is fulfilled: there is a flow over a concave surface.

Application

In practice the applications of this paper are in using the benefits of the Görtler vortices for heat exchange with a liquid enclosed in a rotating cylinder. People have been finding ways for using the benefits of the vortices, like:

- passing air under pressure through a radially-narrow curved duct for purposes of heat exchange [17] A cylinder-analog to such open system is turning the cylinder into an evaporator by introducing an opening at the side far from the motor and placing fins at the down-wash regions on the outside of the cylinder.

- Dr. Forney and Dr. Pierson used the Taylor type setup (Figure 2, Figure 3, and Figure 4) to proto sanitize fresh milk with ultraviolet light [1]. The discovery of fixed along the z-axes down-wash regions allows shining ultra-violet light at the down-wash regions for opaque to ultra violet light liquids, like milk.
- Heating of a liquid inside of a Plexiglas cylinder by laser is also possible by using the intense bubble density at the down-wash regions. The heat exchange mechanism will be Fresnel's losses for power losses for light crossing the boundary of two media with different indexes of refraction, and the intense convective heat exchange at the down-wash regions will prevent melting of the cylinder.
- For using the closed cylinder for a convective exchange with the ambient fluid (air, or other), further study must be done in shapes and lengths of fins and especially in techniques for depositing the fins through the cylinder wall without disturbing the smoothness of the inner surface of the cylinder.

# SUMMARY

The main differences of a flow in a rotating cylinder with flow over a concave surface are: the presence of the Gibbs phenomenon, and the localization in space of the flow front. The suspended pool of water acts like a gravitaional-viscous brake on the Coriolis forces produced by the up- and down-wash regions of the vortices. The gravitational effects by suspended stationary pool of water, for cylinders of a fill-volume fraction more than 7/10, stop the vortices at the point on the bottom of the horizontally-rotating cylinder where the gravitatioinal force is the greatest. That pool is also an analog to the centrifugal force applied by the fluid outside of the boundary layer in a curving duct. This connects this work and the study of flows in a curved duct. We discovered the existence of axiallly-stable down-wash regions in a partially filled horizontally rotating cylinder, for specific narrow intervals of the tangential speed of rotation. This paper's findings were mostly inspired by the theoretical work of H. Görtler and G. Hämmerlin covered in some detail in Chapter 1.

To view videos that support the findings go to: http://www.physics.uco.edu/~dmartin/ , and use the link: "Flows in partially filled horizontally rotating cavities"

# REFERENCES


1. Forney et al., *Systems and methods for disinfection,* WWW Document, ( http://www.patentstorm.us/patents/7507370/description.html ).
2. R. Balmer, "The Hygrocyst-a stability Phenomenon in Continuum Mechanics," Nature, **227**, 600 (1970).
3. *Momentum thickness*, WWW Document, (http://en.wikipedia.org/wiki/Momentum_thickness).
4. L. De Souza , M. de Mendonça, M. de Medeiros, M. Kloker, "Seeding of Görtler vortices through a suction and blowing strip," J. Braz. Soc. Mech. Sci. & Eng. **26** (3), (2004). *http://www.scielo.br/scielo.php?script=sci_arttext&pid=S1678-58782004000300003*.
5. S. Thoroddsen, L. Mahadevan, "Shark-teeth pattern in coating flow inside a horizontally rotating cylinder," Phys. Fluids, **8** (9),S10 (1996). (http://www.seas.harvard.edu/softmat/downloads/pre2000-16.pdf).
6. E. Biedermann, et al., *Unsteady Rimming Flows in Microgravity*, University of Illinois at Urbana-Champaign, 2002, WWW Document, (http://floatn.ec.uiuc.edu/projects/2001_2002/Final_Report2002.doc).
7. H. Wielandt, "Das Iterationsverfaherns bei nicht sebstajungierten Eigenwertaufgaben," Math. Zschr., **50**, 93–143 (1944), WWW Document, (http://gdz.sub.uni-goettingen.de/dms/load/img/?IDDOC=172347

8. H. Görtler, “Dreidimensionales zur Stabilitätstheorie laminarer Grenzschichten,” Z. angew. Math. Mech., **35** (9/10), 362-363 (1955).

9. H. Görtler, “On a three-dimensional instability of laminar boundary layers on concave walls,“ NACA Techn. Mem. 1375, June 1954.

10. G. Hämmerlin, “Uber das Eigenwertproblem der Dreidimensionalen Instabilität Laminarer Grenzschichten an Konkaven Wänden,” Indiana Univ. Math. J. **4** (2), 279–321 (1955), WWW Document, (http://www.iumj.indiana.edu/IUMJ/FULLTEXT/1955/4/54010).

11. H. Schlichting, *Boundary Layer Theory*, 6th ed. (McGraw-Hill, 1968).

12. W. Schmeidler, *Integralgleichungen mit Anwendungen in Physik und Techik*, (Akademische Verlagsgesellschaft Geest & Portig, Leipzig, 1955).

13. G. Taylor, ″Stability of a Viscous Liquid Contained between Two Rotating Cylinders,” Phil. Trans. R. Soc. Lond. A, **223**, 289 (1923).

14. S. Thoroddsen, L. Mahadevan, “Experimental study of coating flows in a partially-filled horizontally rotating cylinder,” Exp. Fluids, **23**, 473-480 (1997), WWW Document, (http://www.seas.harvard.edu/softmat/downloads/pre2000-13.pdf).

15. F. Wortmann, in *Proceedings of XI. International Congress on Applied Mechanics, Munich, 1964,* p. 815.

16. Z. Abdelfattah, A. Bottaro, ”Görtler vortices with system rotation: Linear,” Physics of Fluids A., **5** (5), 1206 (1993).

17. P. McCormack, H. Welker, M. Kelleher, “Taylor- Görtler vortices and their effect on heat transfer,” J. Heat Transfer, **92**, 101-112 (1970).

18. *Viscosity*, WWW Document, (http://wiki.xtronics.com/index.php/Viscosity).

19. *Fourier Series*, WWW Document, (http://www.cage.curtin.edu.au/mechanical/info/vibrations/).

20. *Dynamik der Fluide*, WWW Document, (http://www.kgroesner.de/portrait/english/index1.html).

21. D. Benson, *Music, a Mathematical Offering*, (Cambridge University Press, 2007).

22. *Gibbs Phenomenon*, WWW Document, (http://webcache.googleusercontent.com/search?q=cache:rsE0VZR7crYJ:en.wikipedia.org/wiki/Gibbs_phenomenon+gibbs+phenomenon+low+pass+filter&cd=1&hl=en&ct=clnk&gl=us).

23. D. Sumner, J. L. Heseltine, O. J. P. Dansereau, "Wake structure of a finite circular cylinder of small aspect ratio," Experiments in Fluids,37 (5), 720-730, 2004, WWW Document, (http://www.springerlink.com/content/mdpbl3lgudf2dnv0/).

24. Z. Abdelfattah, A. Bottaro, "Görtler vortices with system rotation: Linear," Physics of Fluids A., **5** (5), 1206 (1993).

25. *Functional,* WWW Document, (http://en.wikipedia.org/wiki/Functional_%28mathematics%29#Integral ).

26. H. Schlichting, "Ueber die Entstehung der Turbulenz in einem rotierenden Zylinder," Nachrichten von der Gesellschaft der

Wissenschaften zu Göttingen, 160-198 (1933), WWW Document, (http://gdz.sub.uni-goettingen.de/dms/load/img/?IDDOC=64234).

27. Görtler, H, "Ueber den Einfluss der Wandkrümmung auf die Entstehung der Turbulenz," Zeits. angew. Math. Mech, **20**, 138-174 (1940).